

A review on statistical noise models for Magnetic Resonance Imaging¹

1

Santiago Aja-Fernández

LPI, ETSI Telecomunicación, Universidad de Valladolid, Spain

Email: sanaja@tel.uva.es

Antonio Tristán-Vega

LPI, ETSI Telecomunicación, Universidad de Valladolid, Spain

Email: atriveg@lpi.tel.uva.es

Abstract

Many image processing applications within MRI are grounded on stochastic methods based on the prior knowledge on the statistics of noise. The ubiquitous Gaussian model provides a poor fitting for medium-low SNRs, yielding to the use of Rician statistics: the noise in MRI has been traditionally modeled as a stationary process governed by a Rician distribution with constant noise power at each voxel. Modern MRI systems turn this model questionable, making it necessary to develop into more complex patterns. We aim at comprehensively reviewing the main statistical rationales and formulations for the noise in MRI lately found in the literature. We attend to three different criteria: the first-order, voxel-wise probability law, the possible spatial variability of the parameters of such distribution, and the possible noise interdependences between neighboring voxels. Several applications using statistical methods are overviewed, discussing the implications each of the models has on them. Finally, we explore the applicability of the surveyed models to some MRI protocols commonly used. Whereas many parallel and nonparallel acquisitions like GRAPPA and SENSE may be fitted into one of the existing models, other nonlinear reconstruction procedures are lacking a proper noise characterization.

Key words: MRI, thermal noise, noise modeling, Rician, non-central Chi, parallel MRI.

INTRODUCTION

Magnetic Resonance (MR) data is known to be affected by several sources of quality deterioration, due to limitations in the hardware, scanning times, movement of patients, or even the motion of molecules in the scanning subject. One source of degradation that affects most of the acquisitions is noise.

The term *noise* in MR can have different meanings depending on the context. For example, it has been applied to degradation sources such as physiological and respiratory distortions in some MR applications and acquisitions schemes (1), (2). Even acoustic sources (the sound produced by the pulse sequences in the magnet) are sometimes referred to as *noise* (3). In this paper we will obviate these issues, focusing on the thermal noise introduced during data acquisition. The principal source of thermal noise in most MR scans is the subject or object to be imaged, followed by electronics noise during the acquisition of the signal in the receiver chain. It is produced by the stochastic motion of free electrons in the RF coil, which is a conductor, and by eddy current losses in the patient, which are inductively coupled to the RF coil.

The presence of noise over the acquired MR signal is a problem that affects not only the visual quality of the images, but also may interfere with further processing techniques such as segmentation, registration or fMRI analysis (4), (5), (6). There are different ways to cope with this degradation, but, due to the random nature of thermal noise, a probabilistic modeling is a proper and powerful solution. The accurate modeling of signal and noise statistics in MR data usually underlies the tools for processing and interpretation within Magnetic Resonance Imaging (MRI).

One of the most direct approaches to cope with acquisition noise in MRI (of course, not the only one) is signal estimation via noise removal. Traditionally, noise filtering techniques in different fields have been based on a well-defined prior statistical model of data, usually a Gaussian model. Noise models in MRI have allowed the natural

¹TECH-LPI2013-01. This work is an original Technical Report of the LPI, Universidad de Valladolid, Spain, Jun. 2013. www.lpi.tel.uva.es/santi. Citation:

S. Aja-Fernández, A. Tristán-Vega, A review on statistical noise models for Magnetic Resonance Imaging, *Tech Report of the LPI*, TECH-LPI2013-01, Universidad de Valladolid, Spain, Jun. 2013. www.lpi.tel.uva.es/santi

extension of many well known techniques to cope with features specific of MRI. Many examples can be found in the literature, such as the Conventional Approach (CA) (4), Maximum Likelihood (ML) (7), linear estimators (8), (9), (10), or adapted non-local mean schemes (11), (12), (13). However, an accurate noise modeling may be useful in MRI not only for filtering purposes, but also for many other processing techniques. For instance, Weighted Least Squares methods to estimate the Diffusion Tensor (DT) have proved to be nearly optimal when the data follows a Rician (14) or a non-central Chi ($nc-\chi$) distribution (15). Other approaches for the estimation of the DT also assume an underlying Rician model of the data: ML and Maximum a Posteriori (MAP) estimation (16), (17), or sequential techniques for online estimation (18), (19) have been proposed. The use of an appropriated noise model is crucial in all these methods to attain a statistically correct characterization of the underlying signals.

Other methods in MRI processing that benefit from relying on a precise noise distribution model include automatic segmentation of regions (20), (21), compressed sensing for signal reconstruction (22), (23), and fMRI activation and simulation (24), (25), (26). All in all, many examples in literature have shown the advantage of statistically modeling the specific features of noise for a specific typology of data.

For practical purposes, it has been usually assumed that the noise in the image domain is a zero-mean, spatially uncorrelated Gaussian process, with equal variance in both the real and imaginary parts. In case the data is acquired by several receiving coils, the exact same distribution is assumed for all of them. As a result, in single coil systems the magnitude data in the spatial domain are modeled using a stationary Rician distribution (5). When multiple (independent) coils are considered and the \mathbf{k} -space is fully sampled, the natural extension of the Rician model yields to a stationary noncentral- χ ($nc-\chi$) distribution (27), whenever the different images are combined using sum of squares, the variance of noise is the same for all coils, and no correlations exist between them.

These two distributions, Rician and $nc-\chi$, have been extensively used in the MR literature whenever a noise model is needed. However, in modern acquisition systems, they may no longer hold as reliable distributions. Interpolations due to non-Cartesian sampling, ghost-correction post-processing for acquisitions schemes such as EPI (28), (29), manufacturer-specific systems for noise and artifacts reduction, or coil uniformity correction techniques will dramatically alter spatial noise characteristics. Thus, in many practical situations, the initial assumptions on the nature of noise do not completely hold. On the other hand, even when these schemes are not used, nowadays MRI systems often collect subsampled versions of the \mathbf{k} -space to speed-up the acquisitions and palliate phase distortions. In order to correct the aliasing artifacts produced by this subsampling, some reconstruction methods are to be used, the so-called Parallel MRI (pMRI) techniques (30), (31). The most popular among them, owing to their common use in commercial devices, are Sensitivity Encoding (SENSE) (32) and GeneRALized Autocalibrated Partially Parallel Acquisitions (GRAPPA) (33), but there are many more, and lots of new emerging ones every day (30), (34).

In this paper we will review the main statistical models commonly used in MRI, under the assumption of a *direct* acquisition, i.e., we will assume that: (1) data are acquired in the \mathbf{k} -space using a regular Cartesian sampling; (2) the different contributions of noise are all independent, so that the total noise in the system is the sum of the noise from each individual source; and (3) post processing schemes such as EPI correction are not applied. Though these assumptions may seem unrealistic for certain applications, they are common in the literature, and otherwise necessary to achieve a reasonable trade-off between the accuracy of the model and its generalization capabilities. Note the corrections mentioned in the previous paragraph are usually manufacturer-dependent or they even depend on the particular magnet devised, hence they will need a more in-depth study which is far from the scope of this paper. In many cases, however, such study can be derived from the general models here described.

With the aforementioned limitations, we present a comprehensive study of the noise models arising in the most common MRI protocols currently used, mainly single- and multiple-coil acquisitions without \mathbf{k} -space subsampling, SENSE, and GRAPPA. In first place we review the popular Rician model as a first order statistical model for the voxel-wise distribution of noise, and introduce the $nc-\chi$ model as a necessary generalization in many multiple-coil systems. pMRI methods require a more careful study, presented in the next section, with the identical conclusion that the $nc-\chi$ generalization is mandatory for GRAPPA. The other widely accepted assumption in noise modeling, i.e., the noise power being constant for the whole image domain, is reviewed next. We reason that a non-stationary behavior must be assumed in many cases due to the inhomogeneous sensitivity of the receiving coils, the existing correlations between the thermal noise produced by each of them, and the reconstruction process itself with GRAPPA. With SENSE, the reconstruction process introduces a different side effect, the spatial correlation of the noise pattern, which is studied in the final part of the manuscript. To conclude, we show the actual relevance of the features studied through representative examples, and discuss their impact over a number of MRI processing pipelines, explaining how

to adapt the existing methods based on stationary Rician noise to more complex models.

FIRST-ORDER STATISTICAL MODELS FOR FULLY SAMPLED SIGNALS

Complex single– and Multiple–Coil MR signals

The \mathbf{k} -space data are acquired in multiple-shot acquisitions through the repeated application of excitation pulses with a different phase encoding gradient for each readout gradient. Each sampled line of the \mathbf{k} -space is frequency encoded, and the measured signal is uniformly sampled at the desired rate. The points in the \mathbf{k} -space measured from the MRI scanner are thus independent samples of the RF signal received by each coil. The primary origin of random fluctuation is the so-called thermal noise (35), whose variance depends on the following parameters:

$$\sigma_{\text{thermal}}^2 \propto 4k_B T R_{\text{eff}} B_W, \quad [1]$$

where k_B is Boltzmann's constant, T is the absolute temperature of the resistor, R_{eff} is the effective resistance of the coil loaded by the object to scan, and B_W is the bandwidth of the noise-voltage detecting system.

Under the assumption that the noise affects equally to all the frequencies, it is independent for each source, and independent on the signal, it can be modeled as a complex Additive White Gaussian Noise (AWGN) process, with zero mean and variance $\sigma_{K_l}^2$ (36), (37):

$$s_l(\mathbf{k}) = a_l(\mathbf{k}) + n_l(\mathbf{k}; 0, \sigma_{K_l}^2(\mathbf{k})), \quad l = 1, \dots, L, \quad [2]$$

with $a_l(\mathbf{k})$ the noise-free signal at the l -th coil (of a total of L coils) and $s_l(\mathbf{k})$ the received (noisy) signal. If the noise in the RF signal is considered stationary, it makes sense to consider n_l itself stationary (which implies that $\sigma_{K_l}^2(\mathbf{k}) = \sigma_{K_l}^2$ is a constant), so that we may write:

$$n_l(\mathbf{k}; 0, \sigma_{K_l}^2(\mathbf{k})) \equiv n_l(\mathbf{k}; 0, \sigma_{K_l}^2) = n_{l_r}(\mathbf{k}; 0, \sigma_{K_l}^2) + j \cdot n_{l_i}(\mathbf{k}; 0, \sigma_{K_l}^2).$$

The complex image domain is obtained as the inverse Discrete Fourier Transform (iDFT) of $s_l(\mathbf{k})$ for each slice and at each coil. Under the assumption that the data is sampled on a Cartesian lattice, and the iDFT is applied without any kind of interpolation/filtering/apodization/zero-padding, the iDFT will be an orthogonal linear transformation, and the noise in the complex image domain will still be Gaussian for each receiving coil:

$$S_l(\mathbf{x}) = A_l(\mathbf{x}) + N_l(\mathbf{x}; 0, \sigma_l^2), \quad l = 1, \dots, L, \quad [3]$$

where $N_l(\mathbf{x}; 0, \sigma_l^2) = N_{l_r}(\mathbf{x}; 0, \sigma_l^2) + j \cdot N_{l_i}(\mathbf{x}; 0, \sigma_l^2)$. Since the iDFT is applied to each coil, it will not introduce any correlation *per se*. However, there may be an initial noise correlation between the receiver coils due to electromagnetic coupling (38), (39), (40). As a consequence, the noise pattern in the complex image domain may be seen as a complex multivariate (one variable per coil) AWGN process, with zero mean and covariance matrix Σ (41):

$$\Sigma = \begin{pmatrix} \sigma_1^2 & \sigma_{12}^2 & \cdots & \sigma_{1L}^2 \\ \sigma_{21}^2 & \sigma_2^2 & \cdots & \sigma_{2L}^2 \\ \vdots & \vdots & \ddots & \vdots \\ \sigma_{L1}^2 & \sigma_{L2}^2 & \cdots & \sigma_L^2 \end{pmatrix}, \quad [4]$$

with $\sigma_{ij}^2 = \rho_{ij}^2 \sigma_i \sigma_j$ and ρ_{ij}^2 the coefficient of correlation between coils i -th and j -th. While this coefficient of correlation depends only on the electromagnetic coupling between coils i and j , the variance of noise for each coil may be easily predicted from that in the \mathbf{k} -space (36), (42), (43):

$$\sigma_l^2 = \frac{1}{|\Omega|} \sigma_{K_l}^2, \quad [5]$$

where $|\Omega|$ is the size of the Field of View (FOV), i.e. the number of points used in the 2D iDFT.

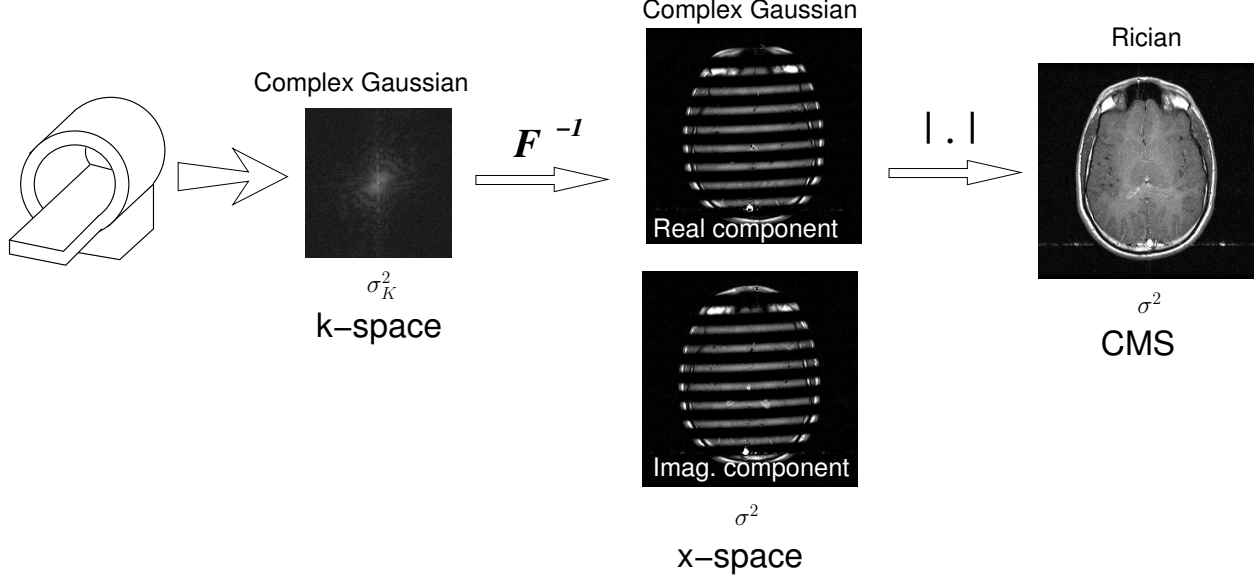


Figure 1. Single-coil acquisition process. The data in both the \mathbf{k} -space and the image domain follow a Gaussian distribution. The final signal after the magnitude is taken will follow a Rician distribution.

Fully sampled single coil: the Rician distribution

For a single-coil acquisition the complex model in eq. [3] simplifies to:

$$S(\mathbf{x}) = A(\mathbf{x}) + N(\mathbf{x}; 0, \sigma^2),$$

with $N(\mathbf{x}; 0, \sigma^2) = N_r(\mathbf{x}; 0, \sigma^2) + j \cdot N_i(\mathbf{x}; 0, \sigma^2)$ a complex AWGN with zero mean and variance σ^2 . The magnitude signal $M(\mathbf{x})$ is the Rician distributed envelope of the complex signal (5):

$$M(\mathbf{x}) = |S(\mathbf{x})|. \quad [6]$$

The probability density function (PDF) of the Rician distribution is defined as (44)¹:

$$p_M(M|A_T, \sigma) = \frac{M}{\sigma^2} \exp\left(-\frac{M^2 + A_T^2}{2\sigma^2}\right) I_0\left(\frac{A_T M}{\sigma^2}\right) u(M), \quad [7]$$

where we call $I_n(\cdot)$ the n -th order modified Bessel function of the first kind, $u(\cdot)$ the Heaviside step function, and $A_T(\mathbf{x}) = |A(\mathbf{x})|$. In the image background, where the SNR is zero due to the lack of water-proton density in the air, the Rician PDF simplifies to a Rayleigh distribution with PDF:

$$p_M(M|\sigma) = \frac{M}{\sigma^2} \exp\left(-\frac{M^2}{2\sigma^2}\right) u(M). \quad [8]$$

For the sake of illustration, a pipeline with the distributions involved in single coil acquisitions is depicted in Fig. 1.

Fully sampled, uncorrelated multiple coils: the noncentral- χ distribution

In a multiple coil system, if the \mathbf{k} -space is fully sampled, the Composite Magnitude Signal (CMS) must be reconstructed from the L complex signals from every coil, $S_l(\mathbf{x})$, with $l = 1 \dots, L$. One of the most used methods is the so-called Sum of Squares (SoS), which can be directly applied over eq. [3] (27), (38):

$$M_L(\mathbf{x}) = \sqrt{\sum_{l=1}^L |S_l(\mathbf{x})|^2}. \quad [9]$$

¹To simplify the notation, the dependency with \mathbf{x} has been removed from the PDFs.

In an ideal scenario the variance of noise is the same for all the coils, which are assumed to produce uncorrelated samples. The covariance matrix Σ in eq. [4] is hence diagonal with identical eigenvalues:

$$\Sigma = \sigma^2 \cdot \mathbf{I},$$

where \mathbf{I} is the $L \times L$ identity and $\sigma^2 = \frac{1}{|\Omega|} \sigma_K^2$. Under these assumptions, $M_L(\mathbf{x})$ follows a noncentral χ (nc- χ) distribution (27), (45) with PDF:

$$p_{M_L}(M_L|A_T, \sigma, L) = \frac{A_T^{1-L}}{\sigma^2} M_L^L \exp\left(-\frac{M_L^2 + A_T^2}{2\sigma^2}\right) I_{L-1}\left(\frac{A_T M_L}{\sigma^2}\right) u(M_L), \quad [10]$$

with $A_T^2(\mathbf{x}) = \sum_{l=1}^L |A_l(\mathbf{x})|^2$. Obviously, for $L = 1$, the nc- χ reduces to the Rician distribution. In the background, this PDF simplifies to a central χ (c- χ) distribution with PDF:

$$p_{M_L}(M_L|\sigma, L) = \frac{2^{1-L}}{\Gamma(L)} \frac{M_L^{2L-1}}{\sigma^{2L}} \exp\left(-\frac{M_L^2}{2\sigma^2}\right) u(M_L), \quad [11]$$

which reduces to Rayleigh for $L = 1$.

Fully sampled, correlated multiple coil: the noncentral- χ approximation

The nc- χ distribution proposed in the previous section has been used to model the noise in MRI when the signals at different receiving coils are combined with SoS (27), (46), (47), (48). However, this CMS will only show nc- χ statistics if the variance of noise is the same for all coils, and no correlation exists between them. Although it is well known that in phased array systems noise correlations do exist (41), (38), (39), (40), this effect is usually left aside due to their minimal effect and practical considerations, as stated in (27).

However, for modern acquisition systems comprising up to 32 or 64 coils, the receivers will show in general a certain coupling. This means that the noisy samples at each \mathbf{k} -space location will be correlated from coil to coil. Assuming such correlation is frequency-independent (i.e. the same for all \mathbf{k} -space samples), the linear iDFT operator will clone this exact same correlation between coils in the complex image domain, so that Σ becomes a non-diagonal, symmetric, positive definite matrix. The off-diagonal elements stand for the correlations between each pair of coils. In this case, the actual PDF is not strictly a nc- χ , though for small correlations it is expected that such model remains approximately valid (49). Even when the nc- χ assumption is feasible, correlations will affect the number of Degrees of Freedom (DoF) of the distribution. If SoS is used, the PDF of the CMS can indeed be accurately approximated with the traditional nc- χ model in eq. [10] whenever effective parameters (reduced L and increased σ) are used (49):

$$L_{\text{eff}}(\mathbf{x}) = \frac{A_T^2(\mathbf{x}) \text{tr}(\Sigma) + (\text{tr}(\Sigma))^2}{\mathbf{A}^*(\mathbf{x}) \Sigma \mathbf{A}(\mathbf{x}) + \|\Sigma\|_F^2}; \quad [12]$$

$$\sigma_{\text{eff}}^2(\mathbf{x}) = \frac{\text{tr}(\Sigma)}{L_{\text{eff}}(\mathbf{x})}, \quad [13]$$

with $\|\cdot\|_F$ the Frobenius norm and $\mathbf{A}(\mathbf{x}) = [A_1(\mathbf{x}), A_2(\mathbf{x}), \dots, A_L(\mathbf{x})]^T$. Note that, with this approximation, the $L_{\text{eff}}(\mathbf{x})$ becomes a non integer number.

Thus, for multiple correlated coils the nc- χ model is just an approximation of the real distribution, and effective parameters must be considered. The parameters of the final distribution are signal-dependent, and therefore they become harder to estimate than simpler models (50).

For the sake of illustration, a pipeline with the distributions involved in multiple-coil acquisitions is depicted on Fig. 2. Note the correlations between coils are the same in both the \mathbf{k} -space and the image domain. These correlations are hardware-dependent and thus inevitable.

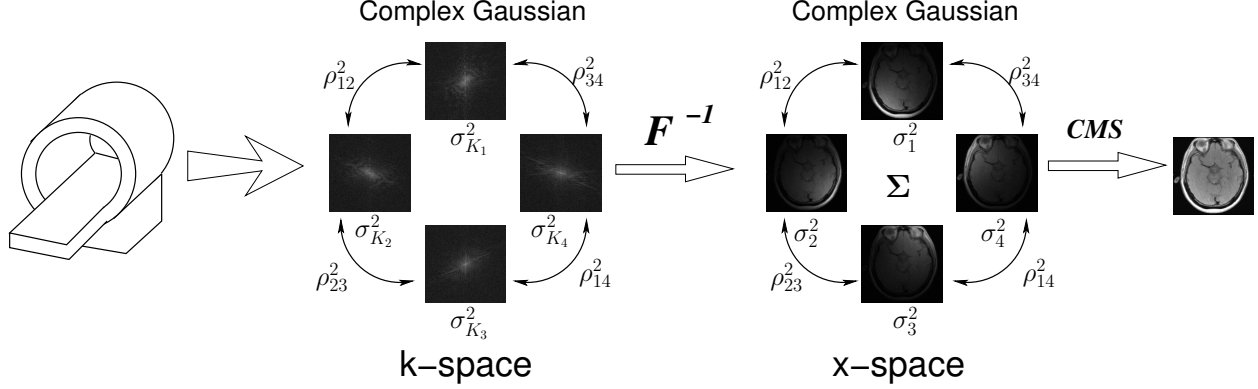


Figure 2. Multiple-coil acquisition process. The data in both the \mathbf{k} -space and the image domain follow a Gaussian distribution in each coil. The final composite magnitude signal will follow different distributions depending on the method employed to aggregate coils and on the possible correlations.

FIRST-ORDER STATISTICAL MODELS FOR PMRI ACQUISITIONS

In the previous section we have reviewed the noise model for multiple-coil systems when the \mathbf{k} -space is fully sampled. However, pMRI protocols usually increase the acquisition rate by subsampling the \mathbf{k} -space data (30), (31), while reducing phase distortions when strong magnetic field gradients are present. The immediate effect of the \mathbf{k} -space subsampling is the appearance of aliased replicas in the image domain retrieved at each coil. In order to suppress or correct this aliasing, pMRI combines the redundant information from several coils to reconstruct a single non-aliased image domain.

The previously presented Rician and nc- χ models do not necessarily hold in this case. Depending on the way the information from each coil is combined, the statistics of the image will follow different distributions. It is therefore necessary to study the behavior of the data for a particular reconstruction method. In this paper we focus on two of the most popular methods, SENSE (32) and GRAPPA (33), in their most basic formulation.

In the following sections we will assume that $s_l^S(\mathbf{k})$ is the subsampled signal at the l -th coil of the \mathbf{k} -space, $S_l^S(\mathbf{x})$ is the subsampled signal in the image domain, and r is the subsampling rate. Since $s_l^S(\mathbf{k})$ is just a subsampled version of the \mathbf{k} -space signal, it is still corrupted with AWGN. If the iDFT is directly applied to the subsampled signal, we will have an AWGN process (43) with variance (compare with eq. [5]):

$$\sigma_l^2 = \frac{r}{|\Omega|} \sigma_{K_l}^2.$$

with $|\Omega|$ the final number of pixels in the FOV. Note the final noise power is greater than in the fully sampled case due to the reduced \mathbf{k} -space averaging, as it will be the case with SENSE (see below). On the contrary, the iDFT may be computed after zero-padding the missing (not sampled) \mathbf{k} -space lines, and then we have (42):

$$\sigma_l^2 = \frac{1}{|\Omega| \cdot r} \sigma_{K_l}^2.$$

In the latter case the noise power is reduced with respect to the fully sampled case, since we average exactly the same number of samples but only 1 of each r of them contributes a noise sample (this will also be the case with GRAPPA), see Table I for a more thorough description. Finally, note that although the level of noise is smaller in GRAPPA due to the zero padding, the SNR does not increase, due to a reduction of the level of the signal.

Statistical model in GRAPPA reconstructed images

GRAPPA estimates the missing lines in a subsampled \mathbf{k} -space by linear interpolation of the complex data (30), (33), (34). While the sampled data $s_l^S(\mathbf{k})$ remain the same, the reconstructed lines $s_l^R(\mathbf{k})$ are estimated through a

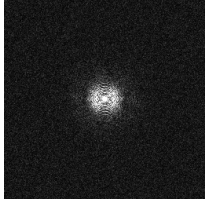

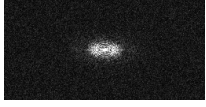

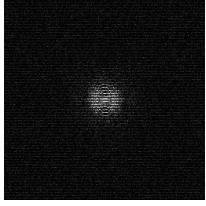
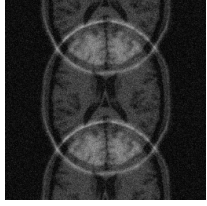
Noise relations			
k-space	Parameters	x-space	Relation
	Fully sampled, $\sigma_{K_l}^2$ k-size: $ \Omega $		$\sigma_l^2 = \frac{1}{ \Omega } \sigma_{K_l}^2$, x-size: $ \Omega $
	Subsampled r , $\sigma_{K_l}^2$ k-size: $ \Omega /r$		$\sigma_l^2 = \frac{r}{ \Omega } \sigma_{K_l}^2$, x-size: $ \Omega /r$
	Subsampled r , $\sigma_{K_l}^2$ k-size: $ \Omega $ (zero padded)		$\sigma_l^2 = \frac{1}{ \Omega \cdot r} \sigma_{K_l}^2$, x-size: $ \Omega $

TABLE I. Relations between the variance of noise in complex MR data for each coil in the **k**-space and the image domain.

linear combination of the existing nearby samples from all the available coils. Given a neighborhood $\eta(\mathbf{k})$ of \mathbf{k} , the interpolation reads:

$$s_l^{\mathcal{R}}(\mathbf{k}) = \sum_{m=1}^L \sum_{\mathbf{c} \in \eta(\mathbf{k})} s_m^{\mathcal{S}}(\mathbf{k} - \mathbf{c}) \omega_{ml}(\mathbf{c}), \quad [14]$$

where $\omega_{ml}(\mathbf{c})$ is a complex coefficient weighting the contribution of the measured signal at the m -th coil in the interpolation of a missing line at the l -th coil, given an offset \mathbf{c} between the measured and the missing samples. These coefficients are learnt from the low-frequency spectrum (as it will show the highest SNR), the so-called Auto Calibration Signal (ACS) lines, which are sampled at the Nyquist rate. Breuer *et al.* in (51) pointed out that eq. [14] can be rewritten using the *convolution* operator:

$$s_l^{\mathcal{R}}(\mathbf{k}) = \sum_{m=1}^L s_m^{\mathcal{S}}(\mathbf{k}) \otimes w_{ml}(\mathbf{k}), \quad [15]$$

where $w_{ml}(\mathbf{k})$ is a convolution kernel that can be easily built from the GRAPPA weights $\omega_{ml}(\mathbf{k})$. For the sake of simplicity in the analysis, these weights are usually considered as constant (non-stochastic). Since a (circular) convolution in the **k**-space is equivalent to a product in the image domain, we can write:

$$S_l^{\mathcal{R}}(\mathbf{x}) = |\Omega| \sum_{m=1}^L S_m^{\mathcal{S}}(\mathbf{x}) \times W_{ml}(\mathbf{x}) \quad [16]$$

$$= \underbrace{|\Omega| \sum_{m=1}^L A_m^{\mathcal{S}}(\mathbf{x}) \times W_{ml}(\mathbf{x})}_{\text{Reconstructed Signal}} + \underbrace{|\Omega| \sum_{m=1}^L N_m(\sigma_n^2) \times W_{ml}(\mathbf{x})}_{\text{Gaussian Noise}} \quad [17]$$

$$= A_l^{\mathcal{R}}(\mathbf{x}) + N_l^{\mathcal{R}}(\mathbf{x}), \quad [18]$$

with $W_{ml}(\mathbf{x})$ the 2D iDFT of $w_{ml}(\mathbf{k})$. This result assumes the signal plus noise model in each coil used in the previous section, a Cartesian sampling of the \mathbf{k} -space, and the GRAPPA weights are considered as constant (non-stochastic). The first important conclusion is that the noise power at each image location \mathbf{x} will be different, since $W_{ml}(\mathbf{x})$ is spatially variant. Since the convolution in eq. [15] is again a linear operator, the noise in the image domain is still an AWGN process. In addition, even assuming that the coils are initially independent, the signals $S_l^R(\mathbf{x})$ will become correlated when the signals from each coil are mixed through $\omega_{ml}(\mathbf{c})$.

The composite magnitude image $M_L(\mathbf{x})$ can be obtained using SoS as shown in eq. [9]. Following a similar reasoning to the one for fully sampled correlated coils, we can conclude that the resultant distribution is not strictly a $nc\text{-}\chi$. Again, it can be modeled as such with a small error if effective values are taken into account (42):

$$L_{\text{eff}}(\mathbf{x}) = \frac{A_T^2 \text{tr}(\mathbf{C}_X^2) + (\text{tr}(\mathbf{C}_X^2))^2}{\mathbf{A}^* \mathbf{C}_X^2 \mathbf{A} + \|\mathbf{C}_X^2\|_F^2}; \quad [19]$$

$$\sigma_{\text{eff}}^2(\mathbf{x}) = \frac{\text{tr}(\mathbf{C}_X^2)}{L_{\text{eff}}}, \quad [20]$$

where $\mathbf{C}_X^2(\mathbf{x}) = \mathbf{W}(\mathbf{x}) \mathbf{\Sigma} \mathbf{W}^*(\mathbf{x})$ is the covariance matrix of the interpolated data at each spatial location; $\mathbf{A}(\mathbf{x}) = [A_1^R(\mathbf{x}), A_2^R(\mathbf{x}), \dots, A_L^R(\mathbf{x})]^T$ is the noise-free reconstructed signal; $A_T^2(\mathbf{x}) = \sum_{i=1}^L |A_i^R(\mathbf{x})|^2$, and $\mathbf{W}(\mathbf{x})$ is a matrix arranged by the set of complex weights $W_{ml}(\mathbf{x})$:

$$\mathbf{W}(\mathbf{x}) = \begin{pmatrix} W_{11}(\mathbf{x}) & W_{12}(\mathbf{x}) & \cdots & W_{1L}(\mathbf{x}) \\ W_{21}(\mathbf{x}) & W_{22}(\mathbf{x}) & \cdots & W_{2L}(\mathbf{x}) \\ \vdots & \vdots & \ddots & \vdots \\ W_{L1}(\mathbf{x}) & W_{L2}(\mathbf{x}) & \cdots & W_{LL}(\mathbf{x}) \end{pmatrix}. \quad [21]$$

The reduced number of DoF in the $nc\text{-}\chi$ model is originated by the correlation and inhomogeneous variance of the complex Gaussians, i.e. by \mathbf{C}_X^2 . In GRAPPA, this artifact mainly comes from the interpolation matrix \mathbf{W} and not from the covariance matrix $\mathbf{\Sigma}$.

Summarizing, the $nc\text{-}\chi$ model does not hold for GRAPPA reconstructed data. However, this distribution can be used as a good approximation of the actual one. For this approximation to hold, effective parameters have to be considered which represent an equivalent, non-subsampled configuration with a smaller number of coils (DoF) and, consequently, a greater level of noise. Note the effective parameters L_{eff} and σ_{eff}^2 are signal dependent (hence spatial-dependent), which is further discussed in the next section.

Statistical model in SENSE reconstructed images

Most of the noise related studies in SENSE are usually done from a SNR or a g-factor (noise amplification) point of view (32), (34). In what follows we present an equivalent reformulation, implicit in previous studies (43), (52), (46) but more coherent with the signal and noise analysis done for the other modalities reviewed in this paper.

For the sake of simplicity, let us assume that SENSE (32) is only be applied to MRI data regularly subsampled by a factor r . The reconstruction takes place in the image domain. Assuming an original size $|\Omega| = M_x \times M_y$, the subsampled signal $S_l^S(\mathbf{x}) = S_l^S(x, y)$ are the (complex) Fourier inverse transform of $s_l^S(\mathbf{k})$, of size $M_x \times (M_y/r)$.

In multiple coil scanners, the image received in coil l -th, $S_l(x, y)$, can be seen as an *original image* $S_0(x, y)$ weighted by the sensitivity of that specific coil:

$$S_l(x, y) = C_l(x, y)S_0(x, y), \quad l = 1, \dots, L \quad [22]$$

An accelerated pMRI acquisition with a factor r will reduce the matrix size of the image at every coil. The signal in one pixel at location (x, y) of l -th coil can be now written as (34):

$$S_l(x, y) = C_l(x, y_1)S_0(x, y_1) + \cdots + C_l(x, y_r)S_0(x, y_r) \quad [23]$$

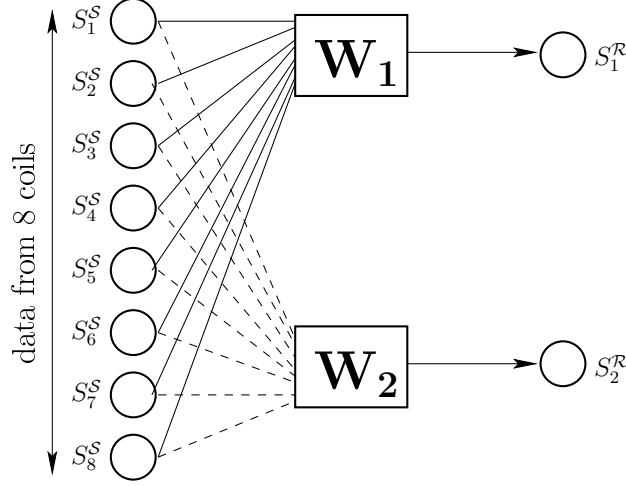


Figure 3. Example of the SENSE interpolation for 8 coils and an acceleration factor $r = 2$.

In SENSE, the reconstructed image $S^{\mathcal{R}}(x, y)$ can be seen as an estimator of the original image $S^{\mathcal{R}}(x, y) = \widehat{S}_0(x, y)$ that can be obtained from eq. (I23). For instance, for $r = 2$ for pixel (x, y) , $S^{\mathcal{R}}(x, y)$ is obtained as

$$\begin{bmatrix} S_1^{\mathcal{R}} \\ S_2^{\mathcal{R}} \end{bmatrix} = \begin{bmatrix} \mathbf{W}_1 & \mathbf{W}_2 \end{bmatrix} \times \begin{bmatrix} S_1^{\mathcal{S}} & \cdots & S_L^{\mathcal{S}} \end{bmatrix}. \quad [24]$$

An example for 8 coils and $r = 2$ is depicted in Fig. 3. In matrix form for each output pixels an arbitrary r

$$S_i^{\mathcal{R}} = \mathbf{W}_i \times \mathbf{S}^{\mathcal{S}} \quad i = 1, \dots, r. \quad [25]$$

$$\mathbf{S}^{\mathcal{R}} = \mathbf{W} \times \mathbf{S}^{\mathcal{S}}, \quad [26]$$

with $\mathbf{W}(x, y) = [\mathbf{W}_1, \dots, \mathbf{W}_r]$ a reconstruction matrix created from the sensitivity maps at each coil. These maps, $\mathbf{C}(x, y) = [\mathbf{C}_1, \dots, \mathbf{C}_L]$ are estimated through calibration right before each acquisition session. Once they are known, the matrix $\mathbf{W}(x, y)$ reduces to a least-squares solver for the overdetermined problem $\mathbf{C}(x, y) \times \mathbf{S}^{\mathcal{R}}(x, y) \simeq \mathbf{S}^{\mathcal{S}}(x, y)$ (32), (34):

$$\mathbf{W}(x, y) = (\mathbf{C}^*(x, y)\mathbf{C}(x, y))^{-1}\mathbf{C}^*(x, y). \quad [27]$$

The correlation between coils may be incorporated in the reconstruction as a pre-whitening matrix for the measurements, and $\mathbf{W}(x, y)$ becomes then a weighted least squares solver with correlation matrix Σ :

$$\mathbf{W}(x, y) = (\mathbf{C}^*(x, y)\Sigma^{-1}\mathbf{C}(x, y))^{-1}\mathbf{C}^*(x, y)\Sigma^{-1}.$$

The SNR of the fully sampled image and the image reconstructed with SENSE are related by the so-called g-factor (52), (34):

$$\text{SNR}_{\text{SENSE}} = \frac{\text{SNR}_{\text{full}}}{\sqrt{r} \cdot g} \quad [28]$$

However, we will focus on the actual noise model underlying the SENSE reconstruction and on the final variance of noise. The final signal for each of the r reconstructed pixels, $S_i^{\mathcal{R}}$, is obtained as a linear combination of the samples in each coil, $S_l^{\mathcal{S}}$, where the noise is Gaussian distributed. Thus, the resulting signal is also Gaussian, with variance:

$$\sigma_i^2 = \mathbf{W}_i^* \Sigma \mathbf{W}_i. \quad [29]$$

Since \mathbf{W}_i is position dependent, i.e. $\mathbf{W}_i = \mathbf{W}_i(x, y)$, so will be the variance of noise, $\sigma_i^2(x, y)$. For further reference, when the whole image is taken into account, let us denote the variance of noise for each pixel in the reconstructed data by $\sigma_{\mathcal{R}}^2(\mathbf{x})$.

Note now that all the lines $S_i^{\mathcal{R}}$ reconstructed from the same data $S_i^{\mathcal{S}}$ will be strongly correlated, since they are basically different linear combinations of the same Gaussian variables. In that case, the covariance between $S_i^{\mathcal{R}}$ and $S_j^{\mathcal{R}}$, $i \neq j$ can be calculated as

$$\sigma_{i,j}^2 = \mathbf{W}_i^* \boldsymbol{\Sigma} \mathbf{W}_j, \quad [30]$$

and the correlation coefficient is derived straight forward:

$$\rho_{i,j}^2 = \frac{\sigma_{i,j}^2}{\sigma_i \sigma_j} = \frac{\mathbf{W}_i^* \boldsymbol{\Sigma} \mathbf{W}_j}{\sqrt{(\mathbf{W}_i^* \boldsymbol{\Sigma} \mathbf{W}_i) (\mathbf{W}_j^* \boldsymbol{\Sigma} \mathbf{W}_j)}}, \quad [31]$$

However, each r correlated lines are far enough within the final image, so we can neglect this correlation effect for processing purposes. In other pMRI modalities that carry out the interpolation in the \mathbf{k} -space, such as GRAPPA, there will also be spatial correlations. However, the iDFT will sparsely distribute them among the entire image domain, considerably reducing their impact when compared to those in \mathbf{x} -space reconstruction methods. Accordingly, they are usually left aside.

All in all, noise in the final reconstructed signal $S^{\mathcal{R}}(\mathbf{x})$ will follow a complex Gaussian distribution. If the magnitude is considered, i.e. $M(\mathbf{x}) = |S^{\mathcal{R}}(\mathbf{x})|$, the final CMS will follow a Rician distribution, just like single-coil systems.

We can summarize our developments as follows:

- 1) Subsampled multi coil MR data reconstructed with Cartesian SENSE follow a Rician distribution at each point of the image.
- 2) The resulting distribution is non-stationary. This means that the variance of noise will vary from point to point across the image.
- 3) The final value of the variance of noise at each point will only depend on the covariance matrix of the original data and on the sensitivity map.
- 4) Each pixel in the final image will be strongly correlated with all those pixels reconstructed from the same original data. Each pixel is correlated with $r - 1$ other pixels. Due to the distance between correlated pixels, this correlation may be left aside.

For the particular case in which there is no initial correlation between coils and all the coils have the same noise variance σ^2 , we can write eq. [29] as:

$$\sigma_i^2 = \sigma^2 \times |\mathbf{W}_i|^2. \quad [32]$$

Since σ^2 is the noise variance of the subsampled data in the image domain, according to eq. [5], it is related to the original noise level without subsampling, say σ_0^2 , by the subsampling rate:

$$\sigma^2 = r \cdot \sigma_0^2,$$

and therefore

$$\sigma_i = \sqrt{r} \cdot \sigma_0 \times |\mathbf{W}_i|, \quad [33]$$

which is totally equivalent to the formulations for SNR reduction in literature (32), (43).

SPATIAL VARIATION OF THE NOISE DISTRIBUTION PARAMETERS: NOISE MAPS

We have concluded in the previous sections that the noise pattern in certain multiple-coil systems may show spatially-variant, or even signal-dependent distributions. The origin of this artifact may be the initial correlation (coupling) between the receiver coils in the MRI scanner, or the reconstruction process in pMRI protocols. In all these cases we are interested in characterizing the variability of the parameters of the noise distribution. From now on, the values of these parameters for each pixel at each coil or in the final CMS will be referred to as *noise maps*.

Noise maps for fully sampled \mathbf{k} -spaces from multiple correlated coils

The existence of correlations between the noise in different coils compels using effective parameters for the $nc\text{-}\chi$ distribution, whose value is given in eq. [13]:

$$\sigma_{\text{eff}}^2(\mathbf{x}) = \frac{\mathbf{A}^*(\mathbf{x}) \boldsymbol{\Sigma} \mathbf{A}(\mathbf{x}) + \|\boldsymbol{\Sigma}\|_F^2}{A_T^2(\mathbf{x}) + \text{tr}(\boldsymbol{\Sigma})}.$$

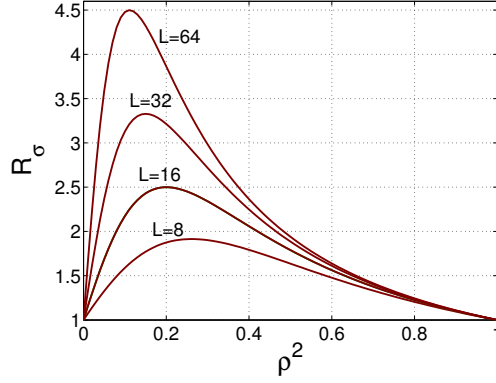


Figure 4. Noise ratio analytically computed for different numbers of coils.

This magnitude depends on the signal itself, hence it is spatially variant, as it is also the case for $L_{\text{eff}}(\mathbf{x})$. This fact makes it very difficult developing statistical models for signal processing. On the other hand, the value of L_{eff} or σ_{eff}^2 is usually not as relevant as the value of their product, $L_{\text{eff}} \sigma_{\text{eff}}^2$ which can be found in some of the moments of the nc- χ .

From eqs. [12] and [13], it is easy to check:

$$L_{\text{eff}}(\mathbf{x}) \cdot \sigma_{\text{eff}}^2(\mathbf{x}) = \text{tr}(\Sigma), \quad [34]$$

which depends now only on Σ . In the particular case in which the variance of noise is equal in each coil :

$$L_{\text{eff}}(\mathbf{x}) \cdot \sigma_{\text{eff}}^2(\mathbf{x}) = L \cdot \sigma^2$$

which is similar to the uncorrelated case.

Hence, the parameter of interest is both signal-independent and spatially-invariant, and building a noise map is worthless. On the contrary, suppose we are interested in the individual value of σ_l^2 . Assuming $\sigma_l^2 = \sigma^2$ is the same for every coil, the effective variance of noise becomes largely different in the background (SNR=0) and signal (SNR $\rightarrow \infty$) areas (49):

- Background: $\sigma_{\text{eff},B}^2 = \sigma^2 (1 + \langle \rho^4 \rangle (L - 1))$.
- Signal: $\sigma_{\text{eff},S}^2 = \sigma^2 (1 + \langle \rho^2 \rangle (L - 1))$.

with $\langle \cdot \rangle$ the sample mean operator, so that:

$$\langle \rho^n \rangle = \frac{1}{L(L-1)} \sum_{i \neq j} \rho_{ij}^n.$$

Since $\rho_{ij}^2 \in [0, 1]$, the effective variance of noise in the signal areas will be greater or equal than in the background, i.e. $\sigma_{\text{eff},S}^2 \geq \sigma_{\text{eff},B}^2$. This reasoning suggests the definition of the noise ratio as:

$$\mathcal{R}_\sigma = \frac{\sigma_{\text{eff},S}^2}{\sigma_{\text{eff},B}^2} = \frac{1 + \langle \rho^2 \rangle (L - 1)}{1 + \langle \rho^4 \rangle (L - 1)} \quad [35]$$

For the sake of illustration, this ratio is depicted in Fig. 4 for different values of the true L and the particular case $\langle \rho^n \rangle = \rho^n$. Even for small values of the correlation coefficient ρ , there is a large variability of σ_{eff}^2 between signal and background areas, which disappears when we consider $L_{\text{eff}} \cdot \sigma_{\text{eff}}^2$.

Noise maps for GRAPPA

Unlike the previous case, the GRAPPA interpolation makes the signal at each coil non-stationary even before SoS is done. According to eq. [17], the noise at the l -th coil in the image domain will follow a complex non-stationary Gaussian distribution, whose noise map for either the real or the imaginary component is defined by:

$$\sigma_l^2(\mathbf{x}) = \mathbf{W}_l^*(\mathbf{x}) \Sigma \mathbf{W}_l(\mathbf{x}), \quad [36]$$

with $\mathbf{W}_l(\mathbf{x}) = [W_{1l}(\mathbf{x}), \dots, W_{Ll}(\mathbf{x})]^T$. If there are no initial correlations between coils, this equation simplifies to:

$$\sigma_l^2(\mathbf{x}) = \sum_{m=1}^L \sigma_m^2 |W_{ml}(\mathbf{x})|^2. \quad [37]$$

This noise map does not depend on the signal, but on the original covariance matrix and on the GRAPPA reconstruction coefficients. Once the SoS is taken, the effective map of noise becomes signal dependent; from eq. [20]:

$$\sigma_{\text{eff}}^2(\mathbf{x}) = \frac{\mathbf{A}^* \mathbf{C}_X^2 \mathbf{A} + \|\mathbf{C}_X^2\|_F^2}{A_T^2 + \text{tr}(\mathbf{C}_X^2)}.$$

If we consider now the product $L_{\text{eff}} \sigma_{\text{eff}}^2$ in the nc- χ distribution, eqs. [19] and [20] show that this parameter is at least signal-independent. As opposed to the fully sampled case, this product is indeed spatially variant, hence it makes sense defining a noise map:

$$L_{\text{eff}}(\mathbf{x}) \cdot \sigma_{\text{eff}}^2(\mathbf{x}) = \text{tr}(\mathbf{C}_X^2(\mathbf{x})).$$

Noise maps for SENSE

After SENSE reconstruction, the final signal follows a non-stationary complex Gaussian, which becomes a Rician when its magnitude is taken. Thus, the same parameters and noise maps can be considered for both. The final noise map will follow eq. [29]:

$$\sigma_i^2(\mathbf{x}) = \mathbf{W}_i^*(\mathbf{x}) \mathbf{\Sigma} \mathbf{W}_i(\mathbf{x}) \quad i = 1, \dots, r.$$

The noise map in SENSE does not depend on the signal, but only on the original covariance matrix and on the sensitivity maps of the coils. This means that, knowing the sensitivity maps and the acceleration rate beforehand, it is possible to predict the output noise map for SENSE.

In addition, note that in the case of SENSE, the noise map is not the only interesting noise-related map to take into account. Due to the reconstruction process, there will be a high correlation between adjacent lines. A correlation map can also be defined following eq. [31].

Some practical examples

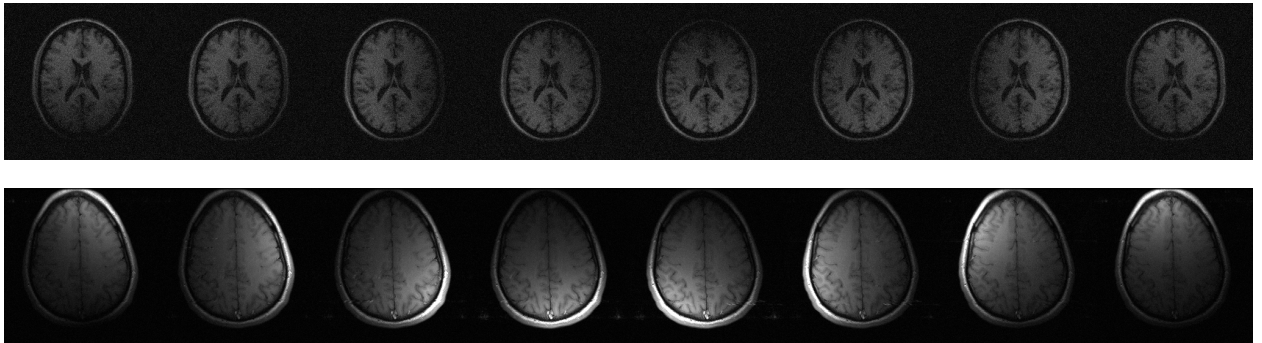


Figure 5. MR data used for illustration: Top: Synthetic 8-coil acquisition with correlated noise. Bottom: Actual brain imaging acquisition from a GE Signa 1.5T scanner with 8 coils.

In this section we will show some of the noise maps previously defined. For the sake of illustration, two different data sets will be considered:

- 1) In order to know before hand all possible parameters such as $\mathbf{\Sigma}$, number of coils, A_i and so on, a synthetic phantom mimicking a parallel acquisition will be used, as shown in Fig. 5. The starting point is a 2D synthetic slice $A_0(\mathbf{x})$ in the image domain from the BrainWeb MR volume (53), with intensity values in $[0, 255]$. The average intensity value for the White Matter is 158, for the Gray Matter is 105, for the cerebrospinal fluid 36 and

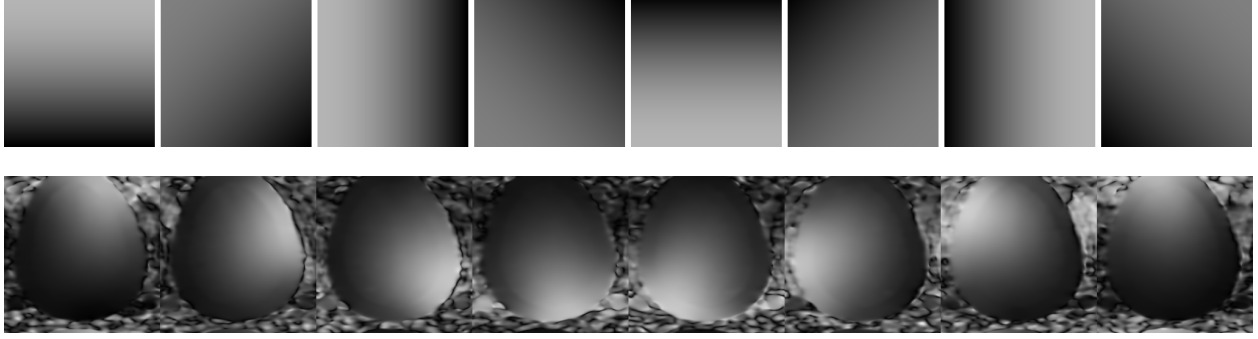


Figure 6. Sensitivity Maps used for the experiments. Top: Synthetic sensitivity map created so that the SoS of the maps gives a constant image. Bottom: Sensitivity map estimated from an actual brain imaging acquisition in a GE Signa 1.5T scanner with 8 coils.

0 for the background. An 8-coil system is simulated using an artificial sensitivity map coded for each coil so that $A_T^2(\mathbf{x}) = \sum_{l=1}^8 |A_l(\mathbf{x})|^2 = A_0(\mathbf{x})$, as shown in Fig. 6 (top). The image domain for each coil is corrupted with complex Gaussian noise with $\sigma_l^2 = 100$ and a correlation coefficient of $\rho^2 = 0.05$ between all coils, so that:

$$\Sigma = 100 \times \begin{pmatrix} 1 & 0.05 & \dots & 0.05 \\ 0.05 & 1 & \dots & 0.05 \\ \vdots & \vdots & \ddots & \vdots \\ 0.05 & 0.05 & \dots & 1 \end{pmatrix}.$$

- 2) A real T1 acquisition of a brain, as shown in Fig. 5, done in a GE Signa 1.5T EXCITE, FSE pulse sequence, 8 coils, TR=500 msec, TE=13.8 msec, image size 256×256 and FOV: 20cm \times 20cm. We will consider the sensitivity maps estimated by the scanning software, see Fig. 6 (bottom).

First we will consider the fully sampled case (FS) for the synthetic data, using SoS to calculate the CMS. Using eq. [12] and eq. [13] we can calculate the maps for $\sigma_{\text{eff}}(\mathbf{x})$ and $L_{\text{eff}}(\mathbf{x})$, we show them in Fig. 7-(a) and 7-(b). There are basically two different areas to take into account: the background area and the signal area. The background has a smaller level of noise than the signal. The product between the two maps is a constant value for the whole image:

$$\sigma_{\text{eff}}^2(\mathbf{x}) \cdot L_{\text{eff}}(\mathbf{x}) = \text{tr}(\Sigma) = \sigma_l^2 \cdot L = 100 \times 8,$$

as shown in Fig. 7-(c). From the same data in each coil, the \mathbf{k} -space is subsampled using an acceleration rate $r = 2$, keeping 32 ACS lines for calibration, and GRAPPA is used for reconstruction. The final CMS is obtained using SoS. Again, we can calculate the maps for noise and number of coils using eq. [20] and eq. [19]. Results for GRAPPA are shown in Fig. 7-(c) and 7-(d). Note that there is a great range of values for $\sigma_{\text{eff}}(\mathbf{x})$, mainly due to the GRAPPA coefficients. Most of the background lies in values around 10, while there are signal areas with levels of noise around 45. In addition, the background and the signal do not show a pattern as regular as the FS case. The product $\sigma_{\text{eff}}^2(\mathbf{x}) \cdot L_{\text{eff}}(\mathbf{x})$ for GRAPPA will not be a constant either, but a map with different values for different \mathbf{x} . The advantage of this product is that it does not depend on the signal, but only on the reconstruction coefficients and on the original covariance matrix. In Fig. 7-(e) we show the map for the synthetic data, and in Fig. 8-(a) the same map is calculated for the real acquisition. For the real acquisition we have just used the GRAPPA coefficients and assumed a Σ matrix like the one in the synthetic experiment. (There are methods allowing the estimation of the actual Σ , but for the sake of illustration and comparison we will consider the same for the two experiments).

Even assuming the same Σ matrix, note that the resultant map differs from the two cases, which gives an idea of the great influence of the GRAPPA coefficients over the final distribution of noise. Using eq. [36] we can also calculate the variance of noise of the complex Gaussian distributions in each coil before the SoS. They are depicted in Fig. 9 (synthetic data) and in Fig. 10 (real acquisition).

Finally, the \mathbf{k} -space is again subsampled using an acceleration rate $r = 2$, and SENSE is used for reconstruction using the sensitivity maps of each of the data sets. Results for $\sigma_{\mathcal{R}}(\mathbf{x})$ and $\rho_{i,j}^2(\mathbf{x})$ are shown in Fig. 7-(f) and 7-(g)(synthetic data) and in Fig. 8-(b) and 8-(c) (real acquisition). Note that the uniformity of the noise map depends

highly on the sensitivity maps. For the synthetic case, the levels of noise take values in a small range. Thus, with a small error, we can assume the noise to be stationary, and work as if it were a single coil acquisition. However, for the real acquisition, the range of values is broader.

DISCUSSION

While many of the features previously discussed for the noise pattern in MRI are well known, many other are not equally familiar to the image processing community. In this section we briefly discuss some important implications of the properties explained before, and provide useful guidelines for the design of image processing pipelines involving the statistical characterization of noise in MRI. The discussion is divided in three blocks corresponding to the voxel-wise (first order) statistics, the spatially variant noise patterns, and the spatial correlations (second order statistics), each of them arising challenging problems in image processing tasks such as image denoising, quantitative diffusion MRI, functional MRI, perfusion MRI, and others.

The Rician and nc- χ models in voxel-wise statistics

The Rician distribution has been widely accepted in the MRI literature as a suitable model for the noise in magnitude images (5). In spite of this, the complexity of Rician statistics has favored the approximation of this distribution with Gaussian functions. This simplification is justified as long as for large SNRs both distributions are virtually identical. The main advantage of the Gaussian approximation relies on the huge background on image processing techniques based on this model. In a statistical sense, Gaussian corrupted signals fulfill two useful properties:

$$E\{M(\mathbf{x})\} = A_T(\mathbf{x}); \quad [38]$$

$$E\{(M(\mathbf{x}) - A_T(\mathbf{x}))^2\} = \sigma^2, \quad [39]$$

i.e. the expected value of the observation equals the magnitude of interest itself, and the expected value of the estimation error does not depend on the actual signal $A_T(\mathbf{x})$. This behavior does not hold for Rician-distributed signals, for which we have:

$$E\{M(\mathbf{x})\} = \sqrt{\frac{\pi}{2}} L_{1/2} \left(-\frac{A_T(\mathbf{x})^2}{2\sigma^2} \right) \sigma, \quad [40]$$

with $L_n(x) = {}_1F_1(-n; 1; x)$, and the estimation error in this case does depend on the actual value of $A_T(\mathbf{x})$. The use of the Gaussian approach to estimate the value $A_T(\mathbf{x})$ will introduce a systematic error (bias) in the estimation, which will decrease when $A_T(\mathbf{x}) \gg \sigma$. Though this bias does not have an impact on the visual assessment of MRI volumes for diagnostic purposes, it will negatively affect quantitative modalities such as diffusion, perfusion, or functional MRI, especially when the SNR is decreased. One very illustrative example is the case of diffusion MRI. In the DWIs image intensities are lower for those gradient directions aligned with the major directions of diffusion. This means that the relevant information is coded in low SNR areas, for which $M(\mathbf{x})$ is systematically greater than $A_T(\mathbf{x})$ and the diffusivity will be underestimated. This effect is even more noticeable in High Angular Resolution DWI (HARDI), where the sensitizing gradients are typically stronger and the SNR is dramatically worsened due to the diffusion-induced attenuation (54).

Many authors have pointed out before this consideration, introducing the Rician statistics in the estimation of diffusion models (17), (55), curve fitting for quantitative perfusion measurements (56), (57), (58), hypothesis tests to assess the activation level in functional MRI (24), (25), or in a preprocessing (denoising) step to get rid of the aforementioned bias for the subsequent processing stages (48), (59), (60), (61). These methods are usually based on non-linear, iterative procedures to recover $A_T(\mathbf{x})$ from $M(\mathbf{x})$ in eq. [40], or they alternatively use the Rician distribution in eq. [7] to estimate $A_T(\mathbf{x})$ from noisy measurements. This complexity can be reduced by alternatively considering the squared magnitude signal, whose relation with the squared original signal is linear (4):

$$E\{M^2(\mathbf{x})\} = A_T^2(\mathbf{x}) + 2\sigma^2.$$

The so-called CA implies the actual signal can be directly computed from the expected value of the squared magnitude signal by simply subtracting the bias term:

$$A_T(\mathbf{x}) = \sqrt{E\{M^2(\mathbf{x})\} - 2\sigma^2}, \quad [41]$$

which has been intensively used in the MRI denoising literature (9), (11), (12), (13), (62).

On the other hand, the nc- χ model is not equally popular in the literature (see Table II), despite of the fact that it has been proved a suitable model for many multiple coils systems, for example those using GRAPPA reconstruction. In these cases, using Rician statistics may lead to great errors (10), (50), and yet a Gaussian distribution might be a preferable model. Nevertheless, for multiple coil systems, both Rician and Gaussian models will cause a certain bias to appear in the estimation of $A_T(\mathbf{x})$, since the expected value of the magnitude signal is not equal to the magnitude to estimate:

$$E\{M_L(\mathbf{x})\} = \sqrt{\frac{\pi}{2}} L_{1/2}^{L-1} \left(-\frac{A_T(\mathbf{x})^2}{2\sigma^2} \right). \quad [42]$$

The biases induced by nc- χ signals are typically larger due to the combined effect of all the Gaussian sources (effective coils), and they are also dramatically increased when the data sets exhibit a poor SNR (15). In this case the CA can be easily extrapolated (50):

$$E\{M_L^2(\mathbf{x})\} = A_T^2(\mathbf{x}) + 2L\sigma^2 \Rightarrow A_T(\mathbf{x}) = \sqrt{E\{M_L^2(\mathbf{x})\} - 2L\sigma^2}, \quad [43]$$

while quantitative methods based on the non-squared magnitude signal for diffusion MRI (17), (55), perfusion MRI (56), (57), (58), functional MRI (24), (25), and others (48), (59), (60), (61) need a deeper reformulation. As a matter of fact, the popular Weighted Least Squares method for diffusion tensor estimation is still usable with nc- χ signals (15). As described in Section II-D, L and σ have to be replaced by their corresponding effective values in case that correlations between coils and/or GRAPPA interpolation are considered (and the nc- χ model becomes then an approximation). This consideration adds an extra layer of complexity to the problem, since neither L_{eff} nor σ_{eff} are known beforehand in general, and they must be estimated. Fortunately, the product $L_{\text{eff}}\sigma_{\text{eff}}^2$ is typically the relevant magnitude, since it accounts for the total amount of noise in the magnitude image instead of the independent contribution of each coil separately. Consider for example eq. [43], which will translate into:

$$A_T(\mathbf{x}) = \sqrt{E\{M_L^2(\mathbf{x})\} - 2L_{\text{eff}}(\mathbf{x}) \cdot \sigma_{\text{eff}}^2(\mathbf{x})} = \sqrt{E\{M_L^2(\mathbf{x})\} - 2\text{tr}(\Sigma)}, \quad [44]$$

Indeed, it is usually simpler estimating $L_{\text{eff}}\sigma_{\text{eff}}^2$ from a noisy data set than it is assessing each of them isolated, in a way that the estimation problem has a similar complexity to the one in the Rician case (although the equations involved are completely different, see the review in (47)).

As an illustration of how a mismatch in the choice of the noise model can affect the estimation, see Fig. 11. 500 samples of two 1D random signals were generated, following a Rician and a (non correlated) nc- χ distribution, with $A_T = 1$ and $\sigma_i = 0.8$. The signal value A_T is estimated using eq. [38], eq. [41] and eq. [44], respectively assuming a Gaussian, Rician and nc- χ model. Note that since we are working in a low SNR scenario, the mismatch between the chosen model and the real data yields to a bias in the estimation of the actual signal value.

Noise non-stationarity and noise maps

The main assumption for single coil Rician acquisitions is that the noise is stationary, and therefore a single value of σ characterizes the whole data set. This premise is extensible to multiple coils systems if the correlations between the receiving coils are neglected. In this case, two unique values of L and σ equally describe the noise properties at all imaged voxels. In case appreciable correlations do exist, however, the model has to be redefined in terms of effective nc- χ parameters that are spatially variant. The noise map for the synthetic example in Fig 7-(a) illustrates the great mismatch of noise values between the signal and background areas. Additionally, L_{eff} and σ_{eff} are not only spatially dependent but also signal-dependent. Fortunately, the product $L_{\text{eff}}\sigma_{\text{eff}}^2$ (the overall noise contribution for all coils) is constant, thus signal-independent, for the whole image domain. As previously stated, this means that most of the quantitative MRI techniques based on local moments computations will be equally valid for single and multiple coils systems whenever fully sampled \mathbf{k} -spaces are acquired. For example, in eq. [44] Σ is a constant.

Parallel reconstructions from partially sampled \mathbf{k} -spaces raise more serious issues. The non-stationarity is even more severe, and signal-dependent artifacts are also present. In this paper we have analyzed the effect of GRAPPA and SENSE over the noise in the final CMS, but a similar study can be carried out for other techniques, such as SMASH,

PILS or non-Cartesian SENSE (30), (34). With SENSE, the noise map mainly depends on the original level of noise and the sensitivity map of each coil. The corresponding map $\sigma(\mathbf{x})$ provides an estimation of how far from the Rician stationary case we are. In the synthetic example previously presented in Fig. 7-(f), for instance, the assumption that σ is constant for the whole image will not produce a great error, while it will considerably simplify the computations.

With GRAPPA, both the initial correlations between coils and the reconstruction interpolation favor the appearance of signal-dependent noise. Contrary to the fully sampled case, considering $L_{\text{eff}}(\mathbf{x}) \cdot \sigma_{\text{eff}}^2(\mathbf{x}) = \text{tr}(\mathbf{C}_X^2(\mathbf{x}))$ will not remove the spatial variability. Even so, $\text{tr}(\mathbf{C}_X^2(\mathbf{x}))$ depends only on Σ and the GRAPPA reconstruction coefficients, so that $L_{\text{eff}}\sigma_{\text{eff}}^2$ is at least signal independent and hence easier to work with (63).

The actual impact of the non-stationarity of noise in quantitative MRI will depend on whether the processing needs a prior estimation of the distribution parameters. For example, ML estimators for Rician PDFs can embed the assessment of σ at each voxel themselves (17). The most of the algorithms for the estimation of diffusion MRI models are run voxel by voxel, and they do not require the actual knowledge of the noise distribution, mainly because they assume an underlying Gaussian distribution of noise (14), (15), (55), (64). In all these cases, the non-stationarity is not a serious issue as long as the computations involve a unique voxel or a neighborhood small enough to consider an approximately homogeneous noise distribution whose parameters are not relevant. On the contrary, other diffusion MRI methods include some sort of spatial regularization, and in this case the spatial variability of noise urges a reformulation (22). In other quantitative methods based on Rician statistics, though they treat each voxel independently, the computations require a prior knowledge of the noise power; hence they will suffer from noise inhomogeneities (24), (25), (56), (57), (58). This is the case also for denoising and other local moments-based techniques (9), (10), (11), (12), (13), (48), (59), (60), (61), (62): local moments are computed as sample estimates in a small neighborhood, mixing up noise samples with different statistical properties. Luckily, noise maps are smooth enough, so that the variability of the distributions parameters can be considered negligible inside those neighborhoods. In any case, the statistical model used for denoising must vary across the image voxels, as it may be checked from one of the simplest cases in eq. [44].

With these considerations, we may conclude that most of the quantitative techniques in MRI may be generalized to the non-stationary case once a proper estimate of the spatial map of distribution parameters is known. Accordingly, the problem of properly estimating $\sigma(\mathbf{x})$ (or $L_{\text{eff}}(\mathbf{x})$ and $\sigma_{\text{eff}}(\mathbf{x})$) earns a capital importance over the remaining applications. Many methods have been proposed for noise estimation, most of them showing a very good performance in terms of accuracy and low variance of the estimates (47). Unfortunately, they usually assume a stationary pattern, hence they do not directly apply to those noise models accounting for non-stationarity.

Certain works have appeared addressing the different properties of noise in signal and background areas (especially when the latter are artificially removed), but they still estimate individual noise parameters for the entire MRI volume (8), (65), (66). Other recent papers estimate non-stationary noise powers in the Rician case (67), (68), though they lack a realistic model for the spatial pattern. An alternative method for the non-stationary nc- χ model (mainly intended for GRAPPA reconstructions) is presented in (63), but it requires knowing the GRAPPA reconstruction coefficients, and only $L_{\text{eff}}(\mathbf{x})\sigma_{\text{eff}}^2(\mathbf{x})$ may be estimated. In case the signal-dependent value of $\sigma_{\text{eff}}^2(\mathbf{x})$ is needed, a proper method must be developed since those previously proposed (47), (48), (65) will fail. In SENSE, the noise maps presented suggest that assuming a constant $\sigma_{\mathcal{R}}$ is not extremely unrealistic in many cases. Even when this simplification is not feasible, if the sensitivity maps are available, a proper noise estimation will not be difficult to make.

As a summary of this section, the traditional noise estimation methods will work “as they are” for single- and multiple-coils systems without subsampling or inter-coil noise correlations. For the other scenarios, some reformulations will be required. We have presented here how to predict the spatial pattern of noise parameters, so that the complexity of noise estimation may be dramatically reduced from the model-free approaches in (67), (68) to a problem where only one degree of freedom has to be estimated. In order to predict the spatial patterns, we need to *a priori* model, for SENSE, the sensitivity maps of each coil (which is inherent to this method), meanwhile with GRAPPA we need to characterize the interpolation weights. Once the maps are derived, local moments-based estimators of noise may be generalized by embedding a regularization step based on the prior knowledge of the spatial patterns.

Spatially correlated noise patterns

In certain situations the noise pattern may exhibit a non-negligible correlation between proximal image locations. With SENSE, every pixel will be highly correlated with another $r - 1$ pixels in the same column, since the interpolation of missing data is performed in the image domain. An illustration is shown in Fig. ?? for $r = 2$. On the contrary,

the interpolation with GRAPPA is performed in the \mathbf{k} -space, where contiguous lines of the spectrum will be equally correlated. However, when the DFT operator is applied to retrieve the image domain, these correlations are sparsely distributed across its support: every line in the image domain is computed as a weighted superposition of all the \mathbf{k} -space lines. Since the DFT weights are highly incoherent, the final correlations may be considered negligible. Of course, these considerations left apart acquisition techniques like EPI, which may represent additional correlation sources.

Whatever the source of the short-term correlations is, the implications in quantitative MRI measurements will be similar. In those procedures involving only point-wise statistics, noise correlations are not much of an issue. For example, if we aim at fitting a perfusion curve (56), (57), (58), it may be done voxel by voxel independently. The same consideration is valid for the most of the diffusion model estimation techniques (14), (55), (64). In the opposite, denoising techniques are almost always grounded on the computation of local moments as in eqs. [41] and [43], see (9), (11), (12), (13), (48), (59), (60), (61), (62). Although the sample estimates of the local moments $E\{M^p(\mathbf{x})\}$ are still valid with correlated samples, their variance (uncertainty) will be drastically increased, compelling the use of larger neighborhoods. However, the size of the estimation neighborhood cannot be arbitrarily increased, since it should be small enough compared to the spatial scale of the relevant features of the MRI volume. The need for estimating the power of noise usually comes together with the denoising filters based on Rician statistics. Histogram-based and local moments-based methods are neither compromised by noise correlations, though once again the uncertainty in the estimation increases and more samples are needed (47). This may be an issue when non-stationarity is considered: the power of noise is a spatially varying magnitude that must be estimated for each voxel from a data set dramatically smaller than the whole support of the image; if the noise samples in such data set are highly correlated, the variance of the estimator could be significantly large, leading to a poor performance of the method.

As a final comment, qualitative (visual) applications of MRI may also be affected by noise correlations: instead of an incoherent noisy pattern that may be easily integrated by the human visual system, noise artifacts will appear as spots whose size depends on the extent of the correlations (with SENSE, the size of the noisy spots will grow proportionally to the acceleration rate). If the size of these spots is comparable to the structures of interest in the MRI volume, this might be an issue.

To sum up, in Table II we summarize some of the different applications in literature that make use of the statistical models reviewed in this paper. Note that, from a practical point of view, most of the authors have assumed a simple Rician model for most applications, while procedures that take into account pMRI statistics are scarce. This gives a global idea of the potential of future research in MRI modeling, since the amount of unfinished problems is still large.

CONCLUSION

The proper modeling of the statistics of thermal noise in MRI is crucial for many image processing and computer aided diagnosis tasks. While the stationary Rician model has been the keystone of statistical signal processing in MR for years, neither the stationarity assumption nor the Rician distribution are always valid. The deviations of the actual statistics of noise with respect to the traditional model will imply very different outcomes depending on the final application, as we describe in the previous section. As a consequence, each application will need a careful choice for a proper and realistic model for the data sets at hand, attending to the need for modeling the actual voxel-wise PDF and/or the spatial distribution of its parameters and possible second-order artifacts (noise correlations).

The existing models for noise statistics surveyed in this paper are suitable for many MRI acquisition sequences, as long as the \mathbf{k} -space is formed by Cartesian sampling, the phase-encoded lines independently acquired, and the image domain retrieved by means of a linear operator. On the contrary, single-shot acquisition sequences like EPI require post-processing schemes, ghost-correction, and others (28), (29). Further post-processing stages may include customary noise reduction systems or corrections to the sensitivity inhomogeneities. In all these cases, large deviations of the noise statistics and the correlation between samples with respect to the AWGN model will appear. This might be the case also for the emerging techniques beyond pMRI, like non-linear GRAPPA (88) or compressed sensing-based reconstructions (89), (90), (91). Even when the \mathbf{k} -space was contaminated with AWGN, the retrieval of the image domain is in these cases heavily non-linear, so that the Rician or nc- χ models are not necessarily appropriate.

Finally, in Table III a survey of the different models reviewed in this paper is carried out.

Model	Application	References
Rician	Signal and noise models	(5), (44), (69)
	Noise Estimation	(7), (8), (37), (47), (70), (71), (72), (73), (74), (66), (65), (67), (75)
	Noise Filtering	(4), (7), (9), (11), (12), (13), (70), (72), (76), (77), (78), (79), (6), (59), (62), (68), (80), (81)
	Segmentation	(20), (21), (37), (82)
	Gaussian Correction	(48), (60), (61), (55)
	Diffusion Tensor Estimation	(14), (16), (18), (19), (23)
	fMRI	(24), (25)
	Perfusion Analysis	(56), (57), (58)
nc- χ	Signal and noise models	(27), (49), (46)
	Noise Estimation	(27), (46), (47), (48), (83), (50)
	Noise Filtering	(10), (48), (84), (85), (50)
	Gaussian Correction	(48), (60)
	Diffusion Tensor Estimation	(15)
GRAPPA	Signal and noise models	(33), (42), (43), (51)
	Noise Estimation	(63), (50)
	Noise Filtering	(50)
SENSE	Signal and noise models	(32), (43), (35)
	Noise Estimation	(86)
	Noise Filtering	(87)

TABLE II. Some examples of usage of the models proposed in this paper. Most of them have been focus of the stationary Rician model.

Composite Magnitude Signal				
Number of coils	Acquisition	Statistical Model	Stationarity	Parameters
1 coil	Single coil	Rician	Stationary	σ^2
Multiple coils (Uncorrelated)	No subsampling + SoS	nc- χ	Stationary	σ^2 L (Number of coils)
Multiple coils (correlated)	No subsampling + SoS	nc- χ (approx.)	Non-stationary	$\sigma_{\text{eff}}^2(\mathbf{x})$ $L_{\text{eff}}(\mathbf{x})$
Multiple coils	pMRI + SENSE	Correlated Rician	Non-stationary	$\sigma_{\mathcal{R}}^2(\mathbf{x})$ $\rho_{i,j}^2(\mathbf{x})$
Multiple coils	pMRI + GRAPPA+ SoS	nc- χ (approx.)	Non-stationary	$\sigma_{\text{eff}}^2(\mathbf{x})$ $L_{\text{eff}}(\mathbf{x})$

TABLE III. Survey of noise models in the final composite magnitude signal for different acquisition schemes.

ACKNOWLEDGMENTS

The authors acknowledge the Ministerio de Ciencia y Educación for Research Grant TEC2010-17982, the CDTI under the cvREMOD project for Research Grant CEN-20091044, the Junta de Castilla y León for grant VA376A11-2.

REFERENCES

1. G. Kruger, G. H. Glover, Physiological noise in oxygenation-sensitive magnetic resonance imaging, *Magn. Reson. Med.* 46 (2001) 1631–637.
2. N. Petridou, A. Schäfer, P. Gowland, R. Bowtell, Phase vs. magnitude information in functional magnetic resonance imaging time series: toward understanding the noise, *Magn. Reson. Imag.* 27 (2009) 1046–1057.
3. A. Counter, A. Olofsson, E. Borg, B. Bjelke, A. Häggström, H. Grahn, Analysis of magnetic resonance imaging acoustic noise generated by a 4.7 t experimental system, *Acta Oto-Laryngologica* 120 (6) (2000) 739–743.
4. G. McGibney, M. Smith, Unbiased signal-to-noise ratio measure for magnetic resonance images, *Med. Phys.* 20 (4) (1993) 1077–1078.
5. H. Gudbjartsson, S. Patz, The Rician distribution of noisy MRI data, *Magn. Reson. Med.* 34 (6) (1995) 910–914.
6. S. Aja-Fernández, M. Niethammer, M. Kubicki, M. E. Shenton, C.-F. Westin, Restoration of DWI data using a Rician LMMSE estimator, *IEEE Trans. Med. Imaging* 27 (10) (2008) 1389–1403.
7. J. Sijbers, A. J. den Dekker, D. Van Dyck, E. Raman, Estimation of signal and noise from Rician distributed data, in: *Proc. of the Int. Conf. on Signal Proc. and Comm.*, Las Palmas de Gran Canaria, Spain, 1998, pp. 140–142.
8. S. Aja-Fernández, C. Alberola-López, C.-F. Westin, Noise and signal estimation in magnitude MRI and Rician distributed images: A LMMSE approach, *IEEE Trans. Image Process.* 17 (8) (2008) 1383–1398.

9. A. Tristán-Vega, S. Aja-Fernández, DWI filtering using joint information for DTI and HARDI, *Med. Imag. Anal.* 14 (2) (2010) 205–218.
10. V. Brion, C. Poupon, O. Riff, J.-F. M. S. Aja-Fernández, A. Tristán-Vega, D. Le Bihan, F. Poupon, Parallel MRI noise correction: an extension of the LMMSE to non central Chi distributions, in: *MICCAI 2011*, Vol. 6891 of *Lecture Notes in Computer Science*, 2011, pp. 217–224.
11. N. Wiest-Daesslé, S. Prima, P. Coupé, S. Morrissey, C. Barillot, Rician noise removal by non-local means filtering for low signal-to-noise ratio MRI: Applications to DT-MRI, in: *Lecture Notes in Computer Science, MICCAI 2008*, 2008, pp. 171–179.
12. J. V. Manjón, J. Carbonell-Caballero, J. J. Lull, G. García-Martí, L. Martí-Bonmatí, M. Robles, MRI denoising using Non-Local Means, *Med. Imag. Anal.* 12 (2008) 514–523.
13. A. Tristán-Vega, V. García-Pérez, S. Aja-Fernández, C.-F. Westin, Efficient and robust Nonlocal Means denoising of MR data based on salient features matching, *Computer Methods and Programs in Biomedicine* 105 (2012) 131–144.
14. R. Salvador, A. Peña, D. K. Menon, T. Carpenter, J. Pickard, E. T. Bullmore, Formal characterization and extension of the linearized diffusion tensor model, *Human brain mapping* 24 (2005) 144–155.
15. A. Tristán-Vega, S. Aja-Fernández, C.-F. Westin, Least squares for diffusion tensor estimation revisited: Propagation of uncertainty with Rician and non-Rician signals, *NeuroImage* 59 (2012) 4032–4043.
16. J. Andersson, Maximum a posteriori estimation of diffusion tensor parameters using a Rician noise model: why, how and but, *NeuroImage* 42 (4) (2008) 1340–1356.
17. B. Landman, P.-L. Bazin, J. Prince, J. Hopkins, Diffusion tensor estimation by maximizing Rician likelihood, in: *Procs. of IEEE 11th International Conference on Computer Vision*, 2007, pp. 1–8.
18. C. Poupon, A. Roche, J. Dubois, J.-F. Mangin, F. Poupon, Real-time MR diffusion tensor and Q-Ball imaging using Kalman filtering, *Med. Imag. Anal.* 12 (5) (2008) 527–534.
19. P. Casaseca-de-la-Higuera, A. Tristán-Vega, S. Aja-Fernández, C. Alberola-López, C. F. Westin, R. San-José-Estépar, Optimal real-time estimation in Diffusion Tensor Imaging, *Magn. Reson. Imag.* 30 (4) (2012) 506–517.
20. X. Wu, S. Bricq, C. Collet, Brain MRI segmentation and lesion detection using generalized gaussian and Rician modeling, in: B. M. Dawant, D. R. Haynor (Eds.), *Medical Imaging 2011: Image Processing*, Vol. 7962, SPIE, 2011, pp. –.
21. S. Roy, A. Carass, P.-L. Bazin, S. Resnick, J. L. Prince, Consistent segmentation using a Rician classifier, *Med. Imag. Anal.* 16 (2) (2012) 524–535.
22. O. Michailovich, Y. Rathi, S. Dolui, Spatially regularized compressed sensing for high angular resolution diffusion imaging, *IEEE Trans. Med. Imaging* 30 (5) (2011) 1100–1115.
23. S. Dolui, A. Kuurstra, O. V. Michailovich, Rician compressed sensing for fast and stable signal reconstruction in diffusion MRI, in: D. R. Haynor, S. Ourselin (Eds.), *Medical Imaging 2012: Image Processing*, Vol. 8314, SPIE, 2012, pp. –.
24. J. Noh, V. Solo, Rician distributed functional MRI: Asymptotic power analysis of likelihood ratio tests for activation detection, in: *Acoustics Speech and Signal Processing (ICASSP)*, 2010 IEEE International Conference on, 2010, pp. 477–480.
25. J. Noh, V. Solo, Rician distributed fMRI: Asymptotic power analysis and Cramer–Rao lower bounds, *IEEE Transactions on Signal Processing* 59 (3) (2011) 1322–1328.
26. M. Welvaert, J. Durnez, B. Moerkerke, G. Verdoolaege, Y. Rosseel, neuRosim: An R package for generating fMRI data, *Journal of Statistical Software* 44 (10).
27. C. Constantinides, E. Atalar, E. McVeigh, Signal-to-noise measurements in magnitude images from NMR based arrays, *Magn. Reson. Med.* 38 (1997) 852–857.
28. M. Stehling, R. Turner, P. Mansfield, Echo-planar imaging: magnetic resonance imaging in a fraction of a second, *Science* 254 (5028) (1991) 43–50.
29. R. L. DeLaPaz, Echo-planar imaging, *Radiographics* 14 (1994) 1045–1058.
30. W. S. Hoge, D. H. Brooks, B. Madore, W. E. Kyriakos, A tour of accelerated parallel MR imaging from a linear systems perspective, *Concepts Magn Reson Part A* 27A (1) (2005) 17–37.
31. D. J. Larkman, R. G. Nunes, Parallel magnetic resonance imaging, *Physics in Medicine and Biology* 52 (2007) 15–55, invited Topical Review.
32. K. P. Pruessmann, M. Weiger, M. B. Scheidegger, P. Boesiger, SENSE: Sensitivity encoding for fast MRI, *Magn. Reson. Med.* 42 (5) (1999) 952–62.
33. M. A. Griswold, P. M. Jakob, R. M. Heidemann, M. Nittka, V. Jellus, J. Wang, B. Kiefer, A. Haase, Generalized autocalibrating partially parallel acquisitions (GRAPPA), *Magn. Reson. Med.* 47 (6) (2002) 1202–1210.
34. M. Blaimer, F. Breuer, M. Mueller, R. Heidemann, M. Griswold, P. Jakob, SMASH, SENSE, PILS, GRAPPA: how to choose the optimal method, *Top Magn Reson Imaging* 15 (4) (2004) 223–236.
35. J. Yu, H. Agarwal, M. Stuber, M. Schär, Practical signal-to-noise ratio quantification for sensitivity encoding: application to coronary MR angiography, *J. Magn. Reson.* 33 (6) (2011) 1330–1340.
36. R. Henkelman, Measurement of signal intensities in the presence of noise in MR images, *Med. Phys.* 12 (2) (1985) 232–233.
37. M. Brummer, R. Mersereau, R. Eisner, R. Lewine, Automatic detection of brain contours in MRI data sets, *IEEE Trans. Med. Imaging* 12 (2) (1993) 153–166.
38. P. Roemer, W. Edelstein, C. Hayes, S. Souza, O. Mueller, The NMR phased array, *Magn. Reson. Med.* 16 (1990) 192–225.
39. C. Hayes, P. B. Roemer, Noise correlations in data simultaneously acquired from multiple surface coil arrays, *Magn. Reson. Med.* 16 (1990) 181–191.
40. M. Harpen, Noise correlations exist for independent RF coils, *Magn. Reson. Med.* 23 (1992) 394–397.
41. R. Brown, Y. wang, P. Spincemaille, R. F. Lee, On the noise correlation matrix for multiple radio frequency coils, *Magn. Reson. Med.* 58 (2004) 218–224.
42. S. Aja-Fernández, A. Tristán-Vega, W. S. Hoge, Statistical noise analysis in GRAPPA using a parametrized non-central chi approximation model, *Magn. Reson. Med.* 65 (2011) 1195–1206.
43. P. Thünberg, P. Zetterberg, Noise distribution in SENSE- and GRAPPA- reconstructed images: a computer simulation study, *Magn. Reson. Imag.* 25 (2007) 1089–94.
44. D. Drumheller, General expressions for Rician density and distribution functions, *IEEE Trans. on Aerospace and Electronic Systems* 29 (2) (1993) 580–588.
45. M. K. Simon, *Probability distributions involving Gaussian random variables*, Kluwer Academic Publishers, 2002.
46. O. Dietrich, J. raya, S. B. Reeder, M. Ingrisch, M. Reiser, S. O. Schoenberg, Influence of multichannel combination, parallel imaging and other reconstruction techniques on MRI noise characteristics, *Magn. Reson. Imag.* 26 (2008) 754–762.

47. S. Aja-Fernández, A. Tristán-Vega, C. Alberola-López, Noise estimation in single- and multiple-coil magnetic resonance data based on statistical models, *Magn. Reson. Imag.* 27 (2009) 1397–1409.
48. C. G. Koay, P. J. Basser, Analytically exact correction scheme for signal extraction from noisy magnitude MR signals, *J. Magn. Reson.* 179 (2006) 317–322.
49. S. Aja-Fernández, A. Tristán-Vega, Influence of noise correlation in multiple-coil statistical models with sum of squares reconstruction, *Magn. Reson. Med.* 67 (2) (2012) 580–585.
50. S. Aja-Fernández, A. Tristán-Vega, V. Brion, Effective noise estimation and filtering from correlated multiple-coil mr data, *Magn. Reson. Imag.* In press.
51. F. A. Breuer, S. A. Kannengiesser, M. Blaimer, N. Seiberlich, P. M. Jakob, M. A. Griswold, General formulation for quantitative g-factor calculation in GRAPPA reconstructions, *Magn. Reson. Med.* 62 (3) (2009) 739–746.
52. P. Robson, A. K. Grant, A. J. Madhuranthakam, R. Lattanzi, D. K. Sodickson, C. A. McKenzie, Comprehensive quantification of snr and g-factor for image-based and k-space-based parallel imaging reconstructions, *Magn. Reson. Med.* 60 (2008) 895–907.
53. D. Collins, A. Zijdenbos, V. Killokian, J. Sled, N. Kabani, C. Holmes, A. Evans, Design and construction of a realistic digital brain phantom, *IEEE Trans. Med. Imaging* 17 (3) (1998) 463–468.
54. D. Jones, P. Basser, Squashing peanuts and smashing pumpkins: how noise distorts diffusion weighted MR data, *Magn. Reson. Med.* 52 (2004) 979–993.
55. R. Clarke, P. Scifo, G. Rizzo, F. Dell’Acqua, G. Scotti, F. Fazio, Noise correction on Rician distributed data for fibre orientation estimators, *IEEE Trans. Med. Imaging* 27 (9) (2008) 1242–1251.
56. O. Friman, A. Hennemuth, H.-O. Peitgen, A Rician-Gaussian mixture model for segmenting delayed enhancement MRI images, in: *Proceedings of the 16th Scientific Meeting of the ISMRM*, Vol. 3, 2008, p. 1040.
57. A. Hennemuth, A. Seeger, O. Friman, S. Miller, B. Klumpp, S. Oeltze, H.-O. Peitgen, A comprehensive approach to the analysis of contrast enhanced cardiac MR images, *IEEE Trans. Med. Imaging* 27 (11) (2008) 1592–1610.
58. V. J. Schmid, B. Whitche, A. R. Padhani, N. J. Taylor, G.-Z. Yang, A Bayesian hierarchical model for the analysis of a longitudinal dynamic contrast-enhanced MRI oncology study, *Magn. Reson. Med.* 61 (1) (2009) 163–174.
59. M. Martín-Fernández, C. Aberola-López, J. Ruiz-Alzola, C.-F. Westin, Sequential anisotropic Wiener filtering applied to 3D MRI data, *Magn. Reson. Imag.* 25 (2007) 278–292.
60. C. G. Koay, E. Özarslan, P. J. Basser, A signal transformational framework for breaking the noise floor and its applications in MRI, *J. Magn. Reson.* 197 (2) (2009) 108–119.
61. M. Martín-Fernández, E. Muñoz-Moreno, L. Cammoun, J.-P. Thiran, C.-F. Westin, C. Alberola-López, Sequential anisotropic multichannel Wiener filtering with Rician bias correction applied to 3D regularization of DWI data, *Med. Imag. Anal.* 13 (1) (2009) 19–35.
62. K. Krissian, S. Aja-Fernández, Noise-driven anisotropic diffusion filtering of MRI, *IEEE Trans. Image Process.* 18 (10) (2009) 2265–2274.
63. S. Aja-Fernández, G. Vegas-Sánchez-Ferrero, A. Tristán-Vega, Noise estimation in MR GRAPPA reconstructed data, in: *2011 IEEE International Symposium on Biomedical Imaging: From Nano to Macro*, 2011, pp. 1815–1818.
64. H.-E. Assemlal, D. Tschumprlé, L. Brun, K. Siddiqui, Recent advances in diffusion MRI modeling: Angular and radial reconstruction, *Med. Imag. Anal.* 15 (4) (2011) 369–396.
65. J. Rajan, D. Poot, J. Juntu, J. Sijbers, Noise measurement from magnitude MRI using local estimates of variance and skewness, *Physics in Medicine and Biology* 55 (16) (2010) N441.
66. R. Maitra, D. Faden, Noise estimation in magnitude MR datasets, *IEEE Trans. Med. Imaging* 28 (10) (2009) 1615–1622.
67. P. Coupé, J. V. Manjón, E. Gedamu, D. Arnold, M. Robles, D. L. Collins, Robust Rician noise estimation for MR images, *Med. Imag. Anal.* 14 (4) (2010) 483–493.
68. J. V. Manjón, P. Coupé, A. Buades, D. L. Collins, M. Robles, New methods for MRI denoising based on sparseness and self-similarity, *Med. Imag. Anal.* 16 (1) (2012) 18–27.
69. A. Macovski, Noise in MRI, *Magn. Reson. Med.* 36 (1996) 494–497.
70. J. Sijbers, A. den Dekker, P. Scheunders, D. Van Dyck, Maximum-likelihood estimation of Rician distribution parameters, *IEEE Trans. Med. Imaging* 17 (3) (1998) 357–361.
71. J. Sijbers, A. den Dekker, J. Van Audekerke, M. Verhoye, D. Van Dyck, Estimation of the noise in magnitude MR images, *Magn. Reson. Imag.* 16 (1) (1998) 87–90.
72. J. Sijbers, A. J. den Dekker, Maximum likelihood estimation of signal amplitude and noise variance form MR data, *Magn. Reson. Imag.* 51 (2004) 586–594.
73. J. Sijbers, A. J. den Dekker, D. Poot, M. Verhoye, N. Van Camp, A. Van der Linden, Robust estimation of the noise variance from background MR data, in: *Proc. of SPIE. Medical Imaging 2006: Image Processing*, Vol. 6144, 2006, pp. 2018–2028.
74. J. Sijbers, D. Poot, A. J. den Dekker, W. Pintjenst, Automatic estimation of the noise variance from the histogram of a magnetic resonance image, in: *Physics in Medicine and Biology*, Vol. 52, 2007, pp. 1335–1348.
75. P. Getreuer, M. Tong, L. Vese, A variational model for the restoration of MR images corrupted by blur and rician noise, in: G. Bebis, R. Boyle, B. Parvin, D. Koracin, S. Wang, K. Kyungnam, B. Benes, K. Moreland, C. Borst, S. DiVerdi, C. Yi-Jen, J. Ming (Eds.), *Advances in Visual Computing*, Vol. 6938 of *Lecture Notes in Computer Science*, Springer Berlin / Heidelberg, 2011, pp. 686–698.
76. R. Nowak, Wavelet-based Rician noise removal for Magnetic Resonance Imaging, *IEEE Trans. Image Process.* 8 (10) (1999) 1408–1419.
77. S. Basu, T. Fletcher, R. Whitaker, Rician noise removal in diffusion tensor MRI, in: *Proceedings of MICCAI*, Vol. 1, 2006, pp. 117–125.
78. P. Coupé, P. Yger, S. Prima, P. Hellier, C. Kervrann, C. Barillot, An optimized blockwise non local means denoising filter for 3D magnetic resonance images, *IEEE Trans. Med. Imaging* 27 (2008) 425–441.
79. T. Marzetta, EM algorithm for estimating the parameters of multivariate complex Rician density for polarimetric SAR, in: *Proc. of ICASSP*, Vol. 5, 1995, pp. 3651–3654.
80. L. He, I. Greenshields, A nonlocal Maximum Likelihood Estimation method for Rician noise reduction in MR images, *IEEE Trans. Med. Imaging* 28 (2) (2009) 165–172.
81. H. Liu, C. Yang, N. Pan, E. Song, R. Green, Denoising 3D MR images by the enhanced non-local means filter for Rician noise, *Magn. Reson. Imag.* 28 (10) (2010) 1485–1496.
82. A. C. S. Chung, J. A. Noble, Statistical 3D vessel segmentation using a Rician distribution, in: *Proceedings of the 2nd MICCAI*, Vol. 1679 of *Lecture Notes in Computer Science*, Springer, 1999, pp. 82–89.
83. C. G. Koay, E. Özarslan, C. Pierpaoli, Probabilistic identification and estimation of noise (PIESNO): A self-consistent approach and its applications in MRI, *J. Magn. Reson.* 199 (1) (2009) 94–103.

84. G. Lohmann, S. Bohn, K. Müller, R. Trampel, R. Turner, Image restoration and spatial resolution in 7-Tesla magnetic resonance imaging, *Magn. Reson. Med.* 64 (1) (2010) 15–22.
85. J. Rajan, J. Veraart, J. V. Audekerke, M. Verhoye, J. Sijbers, Nonlocal maximum likelihood estimation method for denoising multiple-coil magnetic resonance images, *Magn. Reson. Imag.* 20.
86. B. A. Landman, P.-L. Bazin, S. A. Smith, J. L. Prince, Robust estimation of spatially variable noise fields, *Magnetic Resonance in Medicine* 62 (2) (2009) 500–509.
87. A. A. Samsonov, C. R. Johnson, Noise-adaptive nonlinear diffusion filtering of mr images with spatially varying noise levels, *Magnetic Resonance in Medicine* 52 (4) (2004) 798–806.
88. Y. Chang, D. Liang, L. Ying, Nonlinear GRAPPA: A kernel approach to parallel MRI reconstruction, *Magn. Reson. Med.*
89. M. Lustig, D. Donoho, J. Santos, J. Pauly, Compressed sensing MRI, *IEEE Signal Processing Magazine* 25 (2) (2008) 72–82.
90. J. Aelterman, H. Q. Luong, B. Goossens, A. Pizurica, W. Philips, Compass: a joint framework for parallel imaging and compressive sensing in MRI, in: *Proc. International Conference on Image Processing (ICIP'10)*, IEEE, 2010, pp. 1653–1656.
91. M. Lustig, J. Pauly, SPIRiT: Iterative self-consistent parallel imaging reconstruction from arbitrary k -space, *Magn. Reson. Med.* 64 (2) (2010) 457–471.

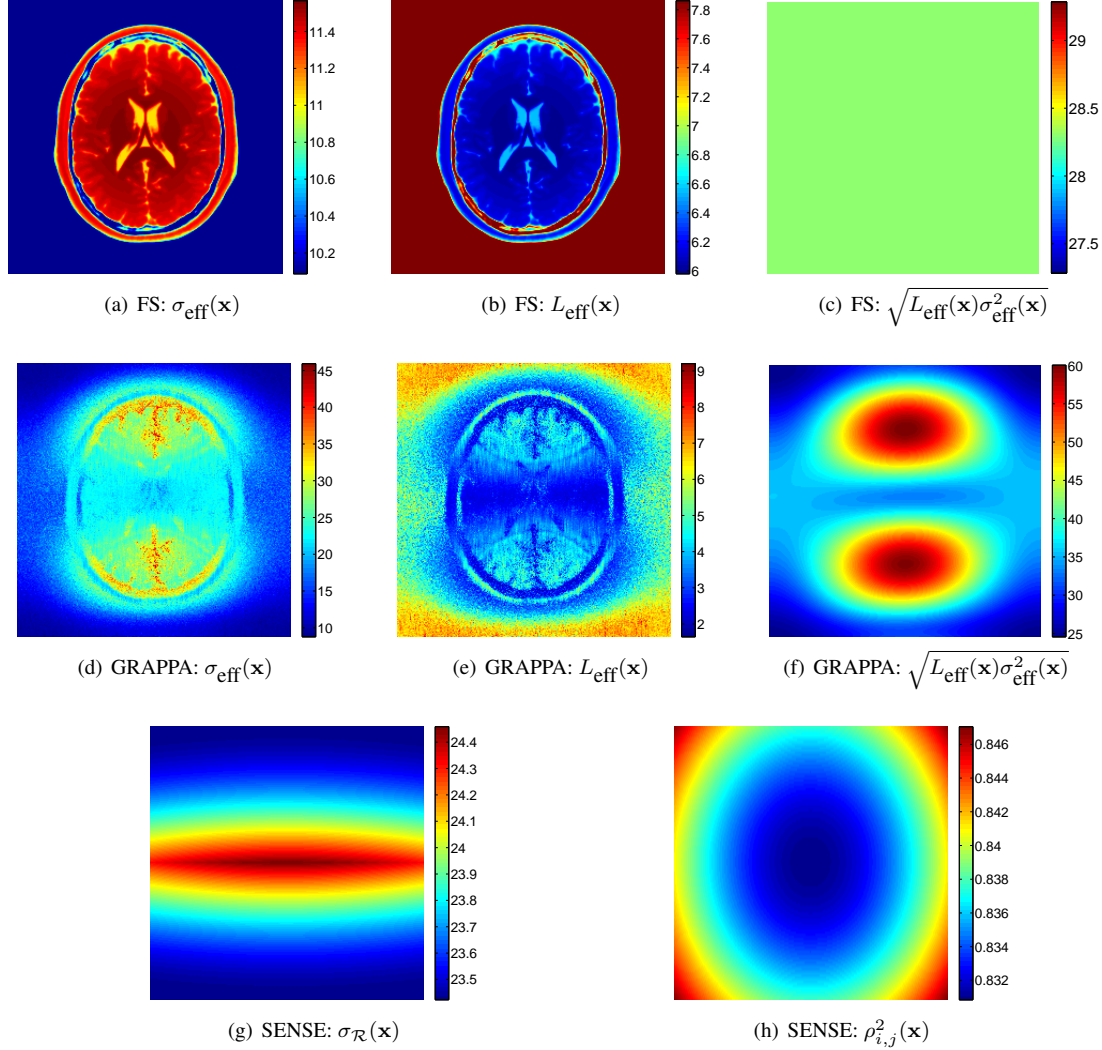


Figure 7. Maps of noise for the synthetic example. (a) Effective noise map for the fully sampled case. (b) Effective number of coils for the fully sampled case. (c) The map of $\sqrt{L_{\text{eff}}(\mathbf{x})\sigma_{\text{eff}}^2(\mathbf{x})}$ for the fully sampled case. (d) Effective noise map for the GRAPPA reconstruction. (e) Effective number of coils for the GRAPPA reconstruction. (f) The map of $\sqrt{L_{\text{eff}}(\mathbf{x})\sigma_{\text{eff}}^2(\mathbf{x})}$ for GRAPPA reconstruction. (g) Noise map for SENSE reconstruction. (h) Coefficient of correlation for the SENSE reconstruction.

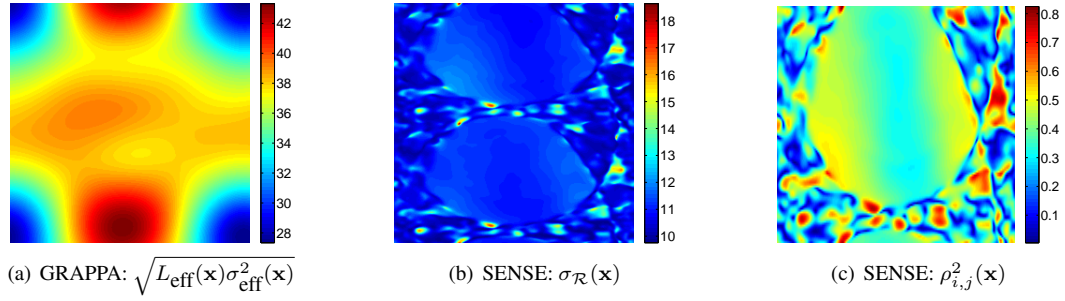


Figure 8. Maps of noise for the real acquisition. (a) The map of $\sqrt{L_{\text{eff}}(\mathbf{x})\sigma_{\text{eff}}^2(\mathbf{x})}$ for GRAPPA reconstruction. (b) Noise map for SENSE reconstruction. (c) Coefficient of correlation for the SENSE reconstruction.

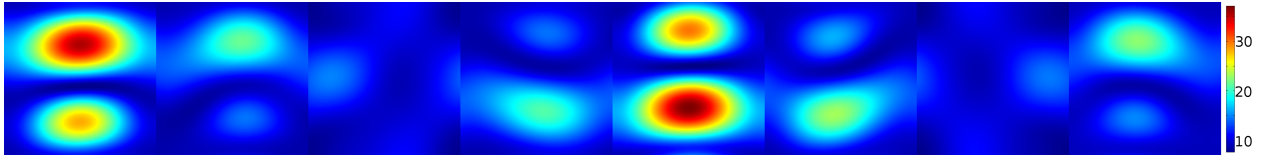


Figure 9. Synthetic example: $\sigma_l(\mathbf{x})$, map of noise in each coil for GRAPPA before SoS.

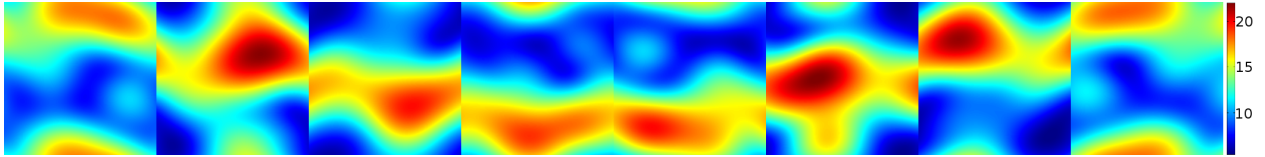


Figure 10. Real acquisition: $\sigma_l(\mathbf{x})$, map of noise in each coil for GRAPPA before SoS.

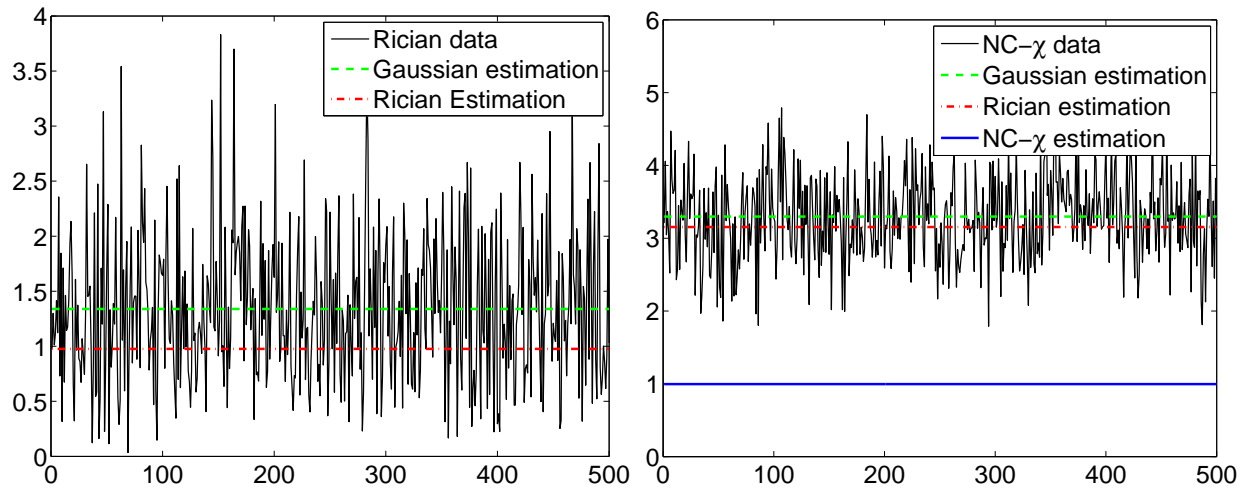


Figure 11. 1D example of estimation of A_T using different models.